CrossMark

Deposition in a changing paleogulf: evidence from the Pliocene–Quaternary sedimentary succession of the Nile Delta, Egypt

Emad Sallam[1] · Bahay Issawi[2] · Refaat Osman[1] · Dmitry Ruban[3]

Abstract

Sedimentary complexes of ancient gulfs provide valuable information about paleoenvironmental dynamics. The study of several Pliocene–Pleistocene sections allowed reconstruction of the regional stratigraphical framework in the southwestern fringes of the Nile Delta. The Kafr El-Shiekh, the Gar El-Muluk, and the Kom El-Shelul formations of the Zanclean Age and the Wastani Formation of the Piacenzian Age constitute the Pliocene sedimentary succession in the study area. The establishment of 11 facies types related to 5 facies associations coupled with the results of the stratigraphical study indicate the existence of a paleogulf corresponding to the modern delta and lower valley of the Nile. This Nile Paleogulf appeared and reached its maximum spatial extent in the beginning of the Pliocene. Then, it retreated gradually and disappeared before the end of this epoch when alluvial sedimentation reestablished. There was significant flux of siliciclastic material to the study area. The Zanclean Flood in the Mediterranean Sea allowed marine incursion in the study area where the river valley incised during the precedent Messinian Salinity Crisis. Regional tectonic uplift and filling of the accommodation space with siliciclastic material from the eroded land were the main controls on the paleogulf evolution. Strengthened glaciation triggered global sea level fall, and alluvial deposition dominated the study area in the late Pliocene–Pleistocene.

Keywords Facies association · Lithostratigraphy · Sediment provenance · Late Cenozoic · Nile Delta

Introduction

The knowledge of paleogeography has progressed significantly during the past decades, but the information on some important and sometimes large features remains restricted. For instance, paleogulfs are known from the geological record, but studies focused on their evolution are few (Dubar 1988; Baloge and

✉ Dmitry Ruban
ruban-d@mail.ru

Emad Sallam
emad.salam@fsc.bu.edu.eg

Bahay Issawi
bissawi@yahoo.com

[1] Department of Geology, Faculty of Science, Benha University, Farid Nada Street 15, Benha 13518, Egypt

[2] Geological Survey of Egypt, Salah Salem Street 3, Abbasyia, Cairo, Egypt

[3] Cherepovets State University, Sovetskiy Avenue 10, Cherepovets, Vologda Region 162600, Russia

Brosse 1993; Negri 2009; Ruban 2010; Pfeiffer et al. 2011; Khonde et al. 2017). An elongated paleogulf penetrating into the African continent generally along the modern Nile Valley is shown on the regional Pliocene–Quaternary paleogeographic map by Guiraud et al. (2005), as well as on the more recent reconstructions of Abdelsalam (2018). The evolution of this feature remains poorly known, although its knowledge would provide some important keys for the understanding of the major Late Cenozoic events (Zachos et al. 2001), the evolution of the Nile River and its delta (Adamson et al. 1980; Woodward et al. 2015; Pennington et al. 2017), and the development of the Cenozoic seaways at the Africa–Arabia connection (Segev et al. 2017).

The latest Miocene–Pliocene sedimentation in northern Egypt was influenced by some major events. For instance, the Messinian witnessed a desiccation of the Mediterranean Sea (Hsü et al. 1973). The change of the base level triggered a huge down-cutting in all river valleys, which once were debouching into the Mediterranean. Gorge-like furrows appeared in North Africa (e.g., Nile gorge and Sahabi channel in Libya; Barr and Walker 1973) and in South Europe (Hsü et al. 1973). The opening of the Gibraltar Strait in the Early Pliocene led to quick reestablishment of the Mediterranean

Sea (Hsü et al. 1973). As a result, water rushing into the above-mentioned gorges formed paleogulfs. Global climate changes in the Late Pliocene (Zachos et al. 2001) led to retreat of the shoreline and dominance of fluvial sedimentation regime on the periphery of Africa.

The present study aims at investigation of stratigraphy, sedimentary facies, and provenance of the Pliocene and Quaternary deposits exposed in the southwestern fringes of the Nile Delta in order to elucidate the changing depositional environments of the Nile Paleogulf. The main objective is the reconstruction of the geological history of the study area and relates the main geological events with global environmental changes.

Geological setting

The study area is located in the southwestern fringes of the Nile Delta (Fig. 1). The Neogene sedimentary succession in the Nile Delta is greatly influenced by structural movements along ENE–WSW fault (hinge zone). This fault subdivided the Nile Delta into two sectors, namely the Northern Delta Embayment and the Southern Delta Block (Harms and Wray 1990).

The sedimentary succession cropping out in the study area ranges in age from the Eocene to the Quaternary (Fig. 2). The Eocene shallow marine limestones (~ 150 m thick) build the high scarps of the Giza Pyramids Plateau. Southward, the Oligocene rocks cover a small area north of Abu Roash and between Tall El-Zalat in the south and Birqash Village in the north. The fluvial and delta sandstones and conglomerates of the Oligocene Gebel Qatrani Formation (18 m thick) overlie unconformably the Eocene strata. The Miocene rocks belong to the Raml Formation that was first described by Vischer (1947). This unit is 40–90 m thick and consists mainly of fluvial sandstones rich in rhizoliths and silicified wood.

The study area is covered by a relatively thick succession of Pliocene (155 m thick) and Quaternary sediments (48 m thick) exposed at many natural outcrops and quarries (Figs. 1 and 2). The Pliocene rocks are widely distributed in the study area as a long narrow belt parallel to the Nile River on its western bank, and they unconformably overlie the Upper Eocene, Oligocene, and Miocene deposits (e.g., Said and Bassiouni 1958; Chumakov 1967, 1968; Abdallah 1970; Chumakov 1973a, b; Hamza 1983; Hamza and Metwally 1984; Abd El Shafy and Metwally 1986; Abd El Shafy et al. 1987; Hamdan 1992; Issawi et al. 2005, 2016, 2018; Issawi and Sallam 2017). The Pliocene deposits are found in isolated hills or small outliers, and dip 10–20° towards the Nile Valley (i.e., to the east) (Said 1962). The Pliocene succession is subdivided into four formations, namely Kafr El-Shiekh, Gar El-Muluk, Kom El-Shelul, and Wastani formations (Fig. 1, Table 1). The Kafr El-Shiekh Formation consists mainly of a thick (80 m) sequence of bluish-black to gray clays. The Gar El-Muluk Formation is composed mainly of gypseous clays (15 m thick) capped by a 5-m

limestone bed bearing brackish-water ostracods and algal filaments. The Kom El-Shelul Formation consists mainly of sandy fossiliferous limestones attaining a thickness of ~ 25 m. The Wastani Formation (~ 22 m) is composed of interbedded cross-bedded sandstone and conglomerate with minor clay intercalations. The Quaternary sediments range in regard to their grain size from clays to conglomerates. Depending on the elevation above sea level, the Quaternary sediments in the study area have been subdivided into the several rock units. Detailed descriptions of the Pliocene and Quaternary units that partly resulted from the new field investigations are given below, together with facies interpretation.

Material and methods

Nineteen stratigraphic sections of Pliocene–Quaternary sediments have been described, measured, and sampled (Fig. 1). The collected material allows to update the lithostratigraphical characteristics of the Pliocene–Quaternary sedimentary packages in the study area. The modern version of the Geological Time Scale adopted by the International Commission on Stratigraphy (Gradstein et al. 2012; Ogg et al. 2016) is followed in the present paper for correct age definition. Macro- and microfossils were picked and identified from the fossiliferous beds for age assignment of the studied rocks (e.g., Fourtau 1920; Blanckenhorn 1921; Hamza 1972; Abd El Shafy and Metwally 1986; Hamdan 1992).

Forty-eight thin sections were prepared and described by using a polarizing microscope. The petrographic description of limestone lithofacies is based on the Dunham's classification scheme (1962) modified by Embry and Kloven (1972). For sandstone description, the classification adopted by Pettijhon et al. (1973) is followed. Facies interpretation and recognition of facies associations are based on the general principles presented by Nichols (2009).

For the purposes of provenance study, 17 sandstone samples were analyzed. After removal of all carbonate and clay fractions, friable sand samples were sifted by using standard sieves. The fine and very fine sand fractions (250–63 μm) were taken for heavy mineral separation. Both heavy and light fractions were separated using bromoform liquid (specific gravity = 2.8), and then these were mounted on a glass slide for microscopic investigation. The relative frequencies of the identified minerals were determined by counting at least 300–350 grains from each sample. The frequency percentages of opaque and non-opaque minerals were calculated.

Results

The results of the present study include updated stratigraphical characteristics and facies interpretations of the Pliocene–
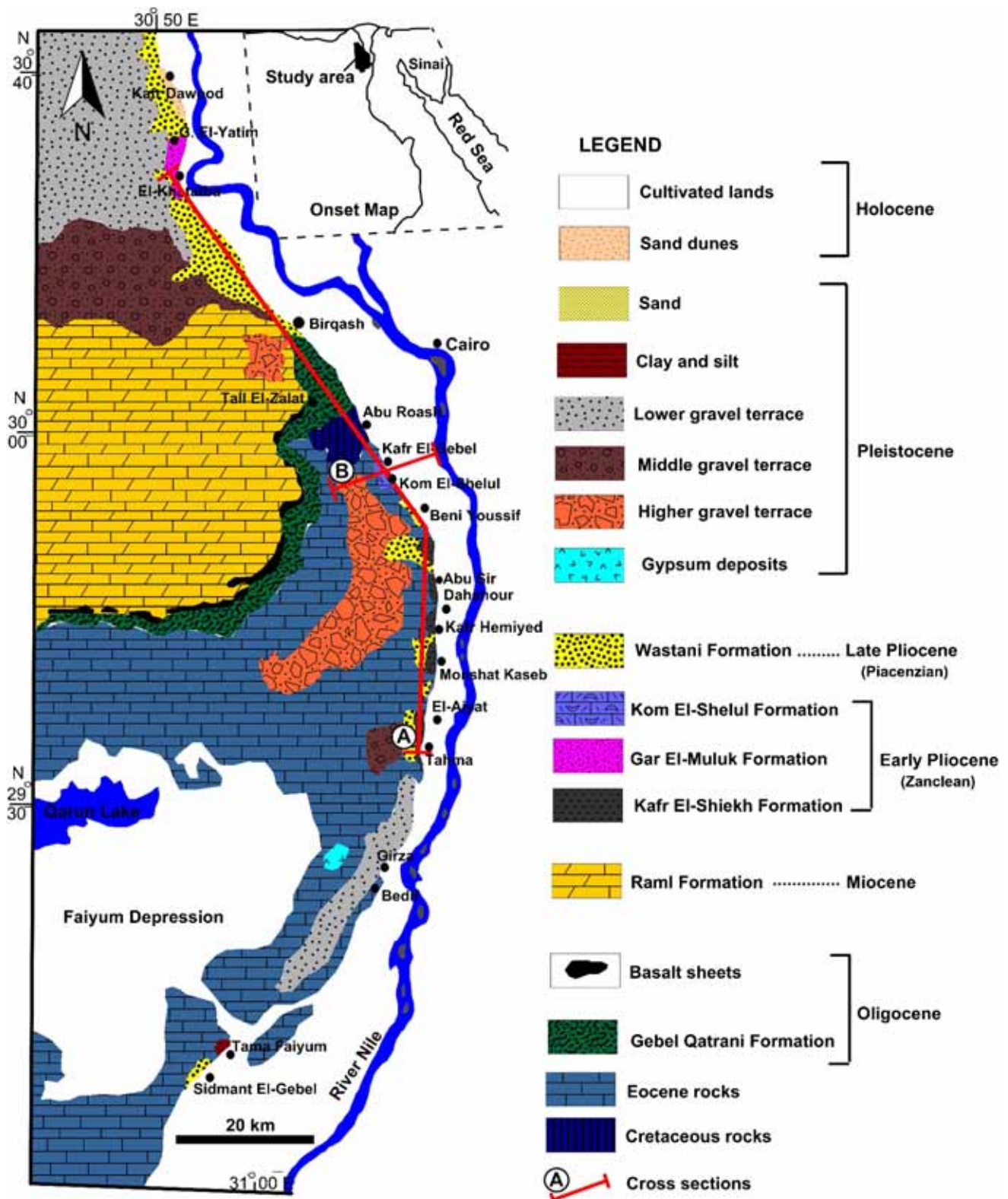
Fig. 1 Geological map of the study area (Geologic Map of Egypt 1981)

Quaternary sedimentary packages of the study area, as well as provenance analysis for the Late Pliocene (Wastani Formation) and Quaternary sands. Five facies associations (FA1–5)

including 11 facies (F-1 to F-11) have been identified in both clastic and carbonate rocks. Facies associations represent outer shelf (FA1: F-1), deltaic to estuarine (FA2: F-2), shallow subtidal

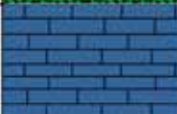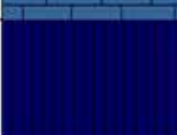| Age		Rock units	Lithology	Lithological description	Microfacies Types (F)	Facies Associations (FA) and palaeoenvironments
Holocene		S.D		Sand dunes	-Sand	Aeolian
Pleistocene		Sand & silt		Sand and silt	-Sand & silt	Aeolian and bars
		Clay & sand		Clay & sand	-Clay & sand	River flood-plain
		LGT		Lower Gravel Terrace	-Clast-supported conglomerate	Channel deposits
		MGT		Middle Gravel Terrace	-Clast-supported conglomerate	Channel deposits
		HGT		Higher Gravel Terrace	-Clast-supported conglomerate	Channel deposits
		Gyp		Gypsum deposits	-Primary gypsum	Saline ponds
Pliocene	Late	Wastani		Coarse sand and conglomerates mostly composed of quartz pebbles cemented by coarse sand and clay	-Cross-bedded sandstone (F-10) -Clast-supported conglomerate (F-11)	Alluvial-dominated (FA5)
		Kom El-Shelul		Fossiliferous coquina limestones: sandy, brownish yellow, hard and rich in Ostrea cucullata. This bed is overlain by calcareous, marly sandstone.	-Bioclastic grainstone (F-3) -Bioclastic packstone (F-4) -Bryzoan wackestone (F-5) -Oyster rudstone (F-6) -Quartz-arenites (F-7) -Quartz-wacke (F-8) -Dolomicrosparite (F-9)	Shallow marine subtidal (FA3) & Intertidal to supratidal (FA4)
	Early	Gar El-Muluk		Clays at base including hard sandstone bands forming protruding ledges within the clay slopes and limestone bed at top	-Clays and laminated algal limestone (F-2)	Transitional deltaic, estuarine (FA2)
		Kafr El-Shiekh		Claystone; bluish black to grey to brownish grey in color, silty, thick-bedded, highly slikinsided, massive, compact and crossed by gypsum veinlets	-Fossiliferous claystone (F-1)	Deep marine to outer shelf (FA1)
Miocene		Raml		Sandstones; white to yellowish white, coarse to medium-grained, poorly sorted, rich in silicified wood		Fluvial-dominated
Oligocene		G. Qatrani		Basalt sheets Variegated sandstones and conglomerate lenses containing petrified tree trunks		Fluvial channels, delta
Eocene		Observatory & Gebel Hof		Fossiliferous, nummulitic limestones		Shallow marine
Cretaceous		Abu Roash		Fossiliferous, oyster limestones		Shallow and open marine

Fig. 2 Lithostratigraphic and facies succession of the study area. Gyp, gypsum deposits; HGT, higher gravel terrace; MGT, middle gravel terrace; LGT, lower gravel terrace; F, facies type; FA, facies association

Table 1 Pliocene rock units of the Nile Valley

Reference	Blanckenhorn (1921)	Hassan et al. (1978)	Issawi et al. (1978)	Abd El Shafy et al. (1987)	Hamdan (1992)	Present study	
Locality	Kom El- Shelul (Giza Pyramids Plateau)	East Beni-Suef	Latitude of Kom Ombo	Nile-Fayium divide	Beni Suef-Faiyum	Southwest Nile Delta	
Pliocene Late	Kom El-Shelul Stufe		Muneiha Formation	Sakkara Shaklufa Formation Formation Kom El-Shelul Formation	Helwan Formation Umm Raqaba Formation Kom El-Shelul Formation	Late	Wastani Formation
Middle Early		Umm Raqaba Formation.				Early	Kom El-Shelul Formation Gar El-Muluk Formation Kafr El-Shiekh Formation

(FA3: F-3–8), intertidal to supratidal (FA4: F-9), and alluvial environments (FA5: F-10, 11).

Updated lithostratigraphy and facies interpretations

Pliocene

The *Kafr El-Shiekh Formation* is exposed between Beni Youssif and Tahma villages forming small isolated patches (Fig. 1). It is composed of a thick sequence of clays (up to 80 m thick), which are bluish-black to gray and brownish-gray in color, silty, thick-bedded, massive, compact, and crossed by gypsum veins (Fig. 3a). The upper part of these clays is laminated and includes sand and gypsum. Sand bodies occur in the form of thin bands or veinlets dissecting clay beds. The sand is yellow to yellowish-white in color and generally medium-grained, and it includes ferruginous iron pockets or nodules. The clays forming the majority of the Kafr El-Shiekh Formation are quarried in many places for building purposes (Fig. 3b).

Along the studied area, the Kafr El-Shiekh Formation varies in thickness and color, and it is unconformably overlain by different younger Pliocene units. To the west of Beni Youssif, the Kafr El-Shiekh Formation is represented by yellow clay at base and black clay at top, and it is covered unconformably by the Kom El-Shelul Formation. To the west of Dahshour, the Kafr El-Shiekh Formation is represented by blackish gray, blocky clay beds (10 m), and it is overlain unconformably by the Wastani Formation. At Monshaat Kaseb, the Kafr El-Shiekh Formation consists of ~ 80 m thick of black clay (bluish-black at base) and includes gypsum veins near top. At Kafr Hemyied, it is represented by 70 m of blackish and bluish-gray clays with sandstone and gypsum intercalations. This package is unconformably overlain by a 2.5-m-thick hard coquina bed belonging to the Kom El-Shelul Formation. In the Tahma area, the formation is represented

by 33 m of dark clays with sand intercalations, and it is overlaid unconformably by the Wastani Formation.

The micropaleontological investigation of the Kafr El-Shiekh clays revealed a rich planktonic foraminiferal assemblage, which includes, particularly, *Cibicidoides* cf. *pumilus* Finger and Lipps, *Globorotalia* (*Truncorotalia*) *crassula* Cushman & Stewart, *Elphidium* cf. *macellum* Fichtel and Moll, *Bolivina* sp., *Ammonia* sp., *Boilivina* sp., *Uvigerina* sp., *Cibicides* sp., *Gyroidenoides* sp., *Bukimina* sp., and *Cibicides* sp. This foraminiferal assemblage implies an Early Pliocene (Zanclean) age of the Kafr El-Shiekh Formation.

The Kafr El-Shiekh Formation is represented by deep marine to outer shelf facies association (FA1) and one facies type, namely fossiliferous claystone (F-1) (Fig. 2). Claystones are bluish-black to brownish-gray, massive, thick-bedded, and partly bioturbated. These consist mainly of kaolinite, montmorillonite, and rare illite. It is commonly fossiliferous facies containing rich planktonic foraminiferal assemblages. The presence of well-preserved planktonic foraminifera and black color of claystones indicate deposition below wave base at depths between 20 and 50 m (Tucker 1982). The fine-grained material of black claystones was largely deposited from suspension. With the increasing of organic content claystones take on a darker gray color and eventually become black (Didyke et al. 1978). Given all the mentioned characteristics, the Kafr El-Shiekh Formation accumulated in a deep marine to outer shelf environment (Zaghloul et al. 1979).

The *Gar El-Muluk Formation* (Said 1971) consists of gypseous clays (with some basal sandstone interlayers) with thickness of 15 m. This unit is capped by black and laminated limestones (5 m) bearing brackish-water ostracods and algal filaments. Black ferruginous sandstones with well-rounded quartz grains cemented by iron oxides are commonly intercalated in the limestone sequence. At El-Khatatba Village, the Gar El-Muluk Formation (3 m thick) is overlaid by the Wastani sands or unconformably by Quaternary sand dunes and gravel terraces (Fig. 3c). The middle part of the formation

Fig. 3 Early Pliocene deposits of the study area. **a** The Kafr El-Shiekh Formation covered by the Quaternary deposits (Zawiet Dahshour). **b** Quarrying in the black clays of the Kafr El-Shiekh Formation (Monshaat Kaseb). **c** The Gar El-Muluk Formation covered by the Wastani Formation (El-Khatatba quarry)
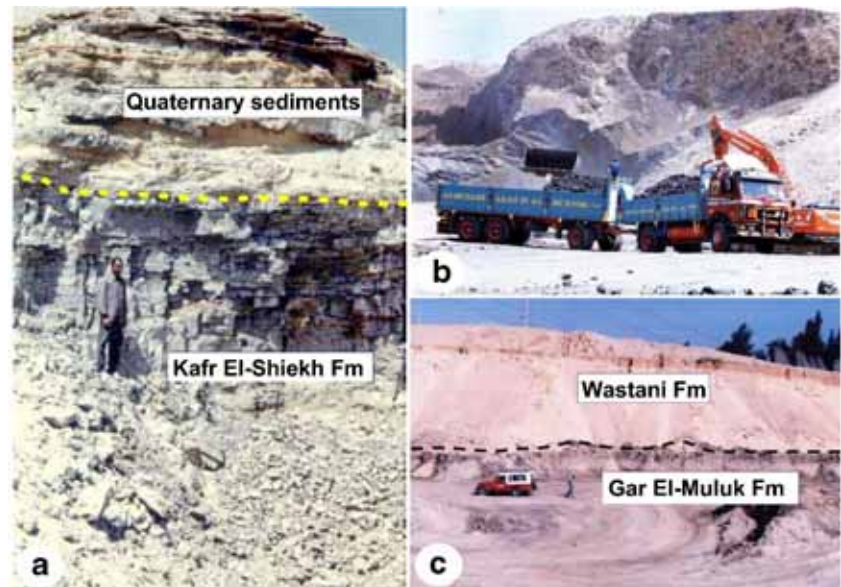
is composed of glauconitic sands including hard, kaolinized sandstone slabs and very thin limestone layers. The fossil content and stratigraphical position of this formation below the Wastani Formation prove its late Early Pliocene (late Zanclean) age (Blanckenhorn 1921; Said 1971).

The Gar El-Muluk Formation is represented by deltaic to estuarine facies association (FA2) and one facies type, namely clays and laminated algal limestone (F-2) (Fig. 2). This facies association consists mainly of gypseous clays including glauconitic sandstones, siltstones, and thin-laminated limestone layers in the middle part. The clays are reddish in color and include medium-grained quartz and calcareous clusters (Fig. 4a). Quartz grains are rounded to subangular and embedded into argillitic groundmass. The occurrence of spineless ostracods, freshwater snails, and algal mats (Fig. 4b) implies short-lived isolated brackish ponds of low gradient margins (Platt and Wright 1992; Huerta and Armenteros 2005; Sallam et al. 2015; Wanas et al. 2015). The presence of glauconitic siltstone may indicate deposition in shallow water, near-shore environment with a very slow rate of sedimentation (Odin and Matter 1981; Odin 1988). The Gar El-Muluk Formation accumulated in humid, near-coast, brackish, deltaic, and transitional non-marine/marine (estuarine) environments originating from short-term oscillations of water level (Flügel 2004). Brackish-water facies of the Gar El-Muluk Formation formed from saline water of the Early Pliocene paleogulf and freshwater of northerly flowing rivers; both debouched in local topographic depressions. These depressions can be observed west of the Nile Delta between Gebel El Yatim (lat. 30° 38′ N, long. 30° 50′ E) and Wadi El-Natrun further west.

The *Kom El-Shelul Formation* is a fossiliferous siliciclastic–carbonate unit attaining a thickness of ~ 25 m. It is exposed between the Faiyum Depression in the south and the Kom El-Shelul area (lat. 29° 55′ N and long. 31° 04′ E) in

the north (Fig. 1). In the Kom El-Shelul area, the Kom El-Shelul Formation is composed of coquina limestones, which are sandy, brownish yellow, hard, and rich in *Ostrea cucullata* Born. Their thickness is ~ 10 m. These limestones are overlain by 2 m of calcareous, marly sandstones rich in *Pecten benedictus* Lamarck, *Chlamys scabrella* Lamarck, and *Xenophora infundibulum* Brocchi forming a marked oyster bank (Fig. 5a). This oyster bank is overlaid by a thin (80 cm) sandstone bed full of *Clypeaster aegyptiacus* Michelin and *Strombus cronatus* Defrance. This unit overlies the older Eocene rocks dipping eastward to the Nile Valley with a marked angular unconformity. To the southwest of Kafr El-Gebel town (Fig. 1), the Kom El-Shelul Formation (~ 11 m thick) dips 15° eastward and overlies the Eocene rocks with a pronounced unconformity surface distinguished by the presence of reworked Eocene limestone boulders (Fig. 5b). Southwards, near the Abu Sir Pyramids, the Kom El-Shelul Formation overlies the black clays of the Kafr El-Shiekh Formation with undulating boundary in-between. Southwest of Beni Youssif (Fig. 1), the Kom El-Shelul Formation is 13.5 m, and it is represented by biostromal limestones full of pelecypod shells with an intercalated conglomerate bed (1.5 m). The conglomerates are made of limestone gravels, pebbles, and fossil fragments embedded into a sandy carbonate matrix. At Kafr Hemyied, the Kom El-Shelul Formation is represented by 11 m of coquina limestones and sandstones changing laterally into more arenaceous and argillaceous lithofacies. Macrofossils collected from the Kom El-Shelul Formation indicate an Early Pliocene (Zanclean) age (Schweinfurth 1889; Mayer-Eymer 1898; Newton 1899; Blanckenhorn 1921; Fourtau 1920; Hamza 1972; Abd El Shafy and Metwally 1986; Hamdan 1992; Issawi et al. 2005).

In the Kom El-Shelul Formation, there are two facies associations (FA3 and FA4) and 7 facies types (F-3–9) (Fig. 2).

Fig. 4 Facies (F-5) recognized in the Gar El-Muluk Formation. **a** Reddish clays including medium-grained quartz and calcareous clusters, P.P.L., X = 33, scale bar = 1 mm. **b** Sparry calcite, P.P.L., X = 33, scale bar = 1 mm
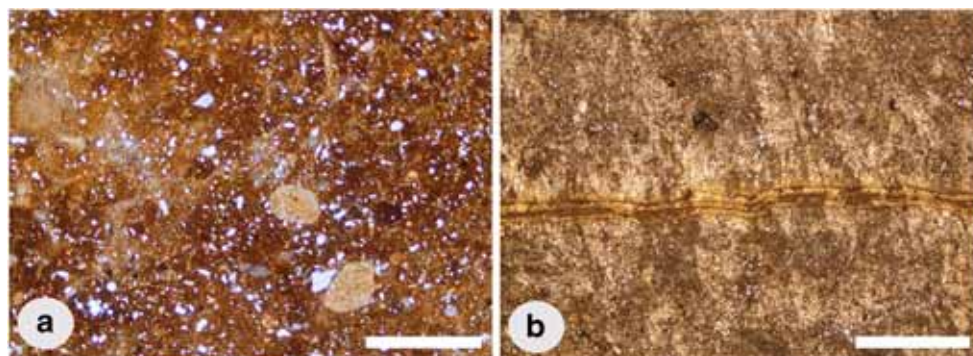
The shallow subtidal marine facies association (FA3) includes six facies types (F-3–8). Sandy bioclastic grainstone (F-3) constitutes gray, grayish-white to yellowish-white ~ 1.5 m limestone beds. More than 90% of grains consist of large skeletal particles including oyster shell fragments with their foliated internal microstructure (Fig. 6a). Some oyster shell fragments are dissolved and recrystallized into granular sparry calcite. There are also abundant echinoid spins and plates with radial shape (Fig. 6b) and well-developed cleavages on their surface (Fig. 6c). Such cleavages may cause fragmentation and break down of echinoid plates (Fig. 6a, c). The outer layer of these plates is preserved as prismatic crystals of calcite or aragonite indicating mixing of freshwater with saline water. A few reworked nummulites with micritized walls (Fig. 6c) and medium to fine-grained detrital quartz grains are also present in a very small amount. The cement consists of fine sparite or granular sparry calcite.

Sandy bioclastic packstone (F-4) is composed of fossiliferous sandy limestones with a thickness of ~ 2.5 m, and is it distinguished by its gray to whitish-gray and yellow colors. This facies consists mainly of skeletal particles and detrital quartz grains (~ 20%) with rare glauconitic pellets embedded into a micritic matrix. Bioclasts are mainly molluscan (bivalve and gastropod) shell fragments, as well as some echinoid fragments. A few reworked nummulites and algal filaments are also observed. Bivalve fragments are mainly oyster shells, which preserve their original composition and retain their foliated internal microstructure that is splitting in some parts. The most important post-depositional process in this facies is neomorphism, which is manifested by recrystallization of bivalve and gastropod shell walls into granular sparry calcite (Fig. 6d–f). The size of calcite crystals often increases away from the shell wall. Shell walls of gastropods were dissolved and replaced by granular sparry calcite while their chambers were filled by fine to medium detrital quartz grains, mostly of monocrystalline type (Fig. 7a).

Sandy bryozoan wackestone (F-5) constitutes yellow to yellowish-gray, sandy, hard, and fossiliferous limestones of ~ 1 m in thickness. This facies consists chiefly of bryozoan fragments, which appear as strings of cells filled with sparite and joined by dark laminated calcite of cracked stems (Fig. 7b). Echinoid plates with their characteristic radial shape and well-developed cleavages are also common in this facies (Fig. 7c). Bivalve shell fragments, gastropods, and a few reworked nummulites are also present (Fig. 7d). Nummulite chambers are highly micritized showing dark mud filling that implies depositional reworking. Non-skeletal components are represented by considerable amount of subangular to subrounded detrital medium sand quartz grains embedded into a lime-mud matrix partially recrystallized to fine sparite.

Sandy oyster rudstone (F-6) is represented by brownish to reddish-brown, sandy, hard fossiliferous coquina limestones of ~ 1.5 m in thickness. This facies is grain-supported and composed mainly of large fragments of oyster shells preserving their original composition and retaining their foliated internal microstructure (Fig. 7e). Medium- to coarse-grained quartz grains embedded into a micritic matrix is also observed. The quartz grains are rounded to subrounded, moderately sorted, and showing undulose wavy extinction. Most of these quartz grains are of monocrystalline type.

Quartz-arenite (F-7) consists mainly of quartz grains (~ 90%). Skeletal particles, heavy minerals (e.g., zircon and tourmaline), glauconite, and flakes of clay minerals are occasional. This facies includes three types based on cement, roundness, and sorting of grains, namely calcareous quartz-arenite, argillaceous quartz-arenite, and fossiliferous quartz-arenite. Calcareous quartz-arenite is composed of monocrystalline, medium- to coarse-grained, rounded to subrounded, moderately sorted quartz grains forming more or less 95% of the rock (Fig. 8a). Calcite is observed in a large amount as intergranular pore-filling cement. Argillaceous quartz-arenite consists of quartz grains forming ~ 92% of the grains (Fig. 8b). Quartz grains are medium- to coarse-grained, subangular to subrounded, showing undulose wavy extinction, and being poorly to moderately sorted. The matrix is argillitic. Fossiliferous quartz-arenite is composed of rounded to subrounded (even subangular), medium- to coarse-sized quartz grains (85%), mostly of monocrystalline type. These grains show undulose wavy extinction, and they are moderately sorted. Bivalve shell fragments and reworked nummulites constitute ~ 10% of the grains (Fig. 8c). The cement is either argillaceous or ferruginous.

Fig. 5 Field photographs of the Kom El-Shelul Formation. **a** Biostromal limestones (F-3) in the middle part of the Kom El-Shelul Formation (Kafr El-Gebel). **b** Boundary contact between the Kom El-Shelul Formation and the underlying Eocene rocks (west of Kafr El-Gebel)
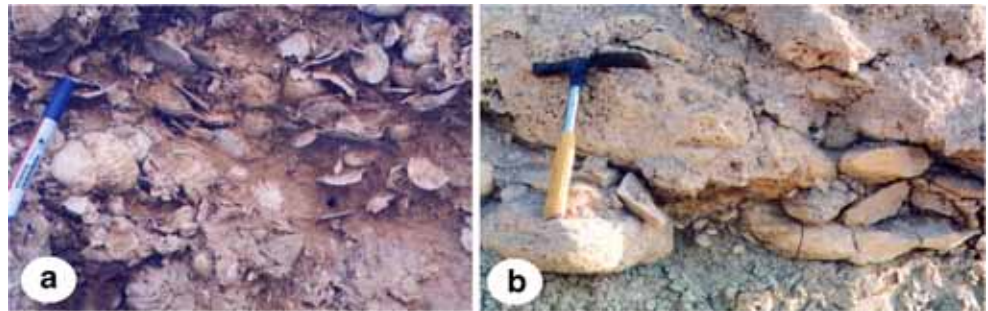
Glauconitic quartz-wacke (F-8) is composed of monocrystalline quartz grains, which are fine- to very fine-grained, subangular, subrounded or rounded, and well-sorted. Detrital, greenish-yellow, fine- to medium-grained, subrounded to rounded glauconite grains are also present (5–10%) indicating slow deposition with many interruptions. The matrix is mainly argillaceous or clayey. Fine-grained rhombic-shape dolomite crystals and quartz grains partly rimmed by silica overgrowths are also present.

In the facies association (FA3: F3–8) described above, the dominance of bioclastic material mixed with detrital glauconitic particles implies a shallow marine depositional environment. Development of bivalve-gastropod wackestone, packstone, grainstone, and rudstone facies permits to assign the F3–8 to normal marine, low-energy, shallow subtidal environment of the platform interior (Wilson 1975; Flügel 2004). The presence of calcareous and fossiliferous quartz-arenite suggests deposition in the near-shore environment with high siliciclastic input.

Fig. 6 Facies types recognized in the Kom El-Shelul Formation. **a** Sandy bioclasts grainstone (F-3) showing oyster shell fragments and fragmented echinoid plate cemented by sparry calcite, P.P.L., X = 33, scale bar = 1 mm. **b** Sandy bioclastic grainstone showing radial shaped echinoid plate and bivalve shell fragment replaced by sparry calcite, P.P.L., X = 33, scale bar = 1 mm. **c** Sandy bioclastic grainstone (F-3) showing well-developed cleavages in echinoid plate and reworked nummulite, P.P.L., X = 33, scale bar = 1 mm. **d** Sandy bioclastic packstone (F-4) showing the neomorphism of the bivalve and gastropod shell walls into sparry calcite, P.P.L., X = 33, scale bar = 1 mm. **e** Sandy bioclastic packstone (F-4) showing the recrystallization of the bivalve shell fragments into granular sparry calcite, P.P.L., X = 33, scale bar = 1 mm. **f** Sandy bioclastic packstone (F-4) showing the recrystallization of the shell fragments into granular sparry calcite, P.P.L., X = 33, scale bar = 1 mm
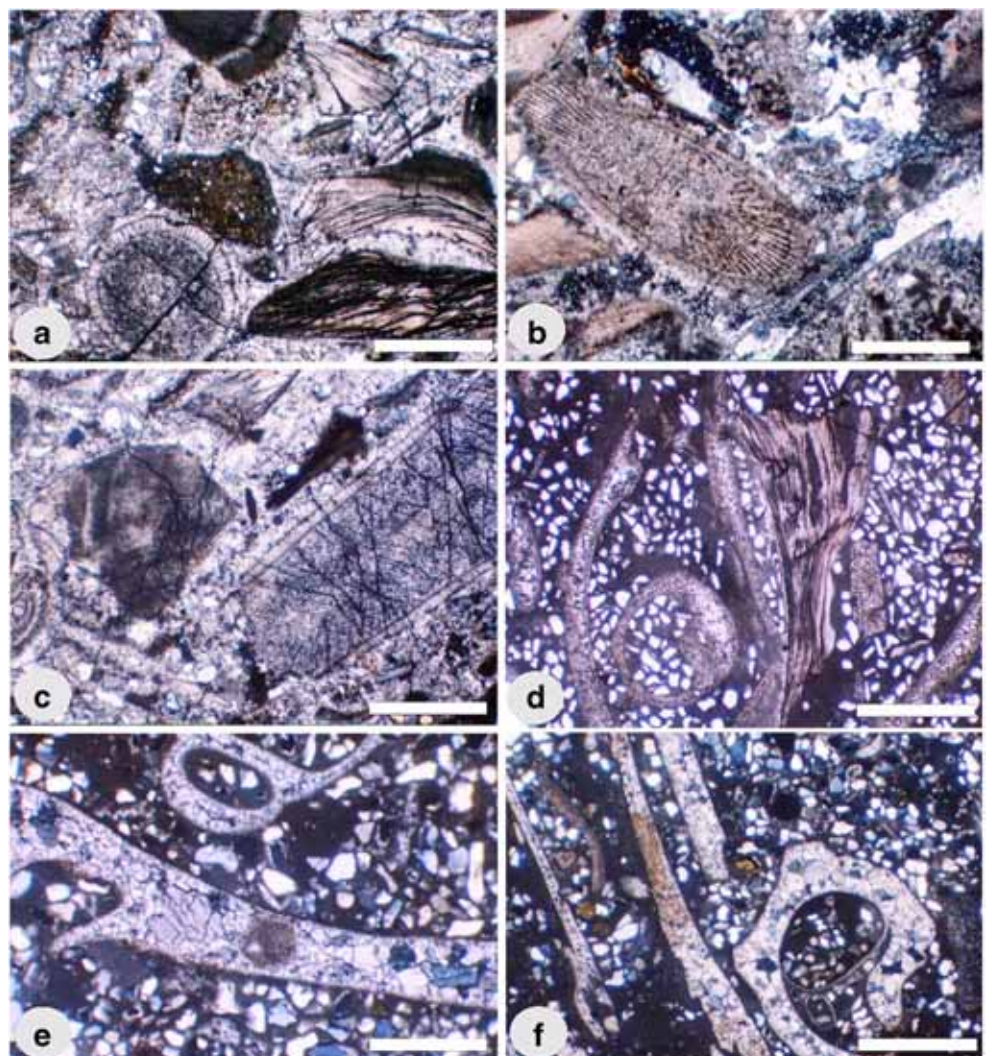
Fig. 7 Facies types recognized in the Kom El-Shelul Formation (continued). **a** Sandy bioclastic packstone (F-4) showing a long section in gastropod shell preserved as sparry calcite; most of chambers are filled with monocrystalline quartz grains, P.P.L., X = 33, scale bar = 1 mm. **b** Sandy bryozoan wackestone (F-5), P.P.L., X = 33, scale bar = 1 mm. **c** Echinoid plate (F-5) with radial shape and well-developed cleavages, P.P.L., X = 33, scale bar = 1 mm. **d** Sandy nummulitic wackestone (F-5), P.P.L., X = 33, scale bar = 1 mm. **e** Sandy oyster rudstone (F-6), P.P.L., X = 33, scale bar = 1 mm
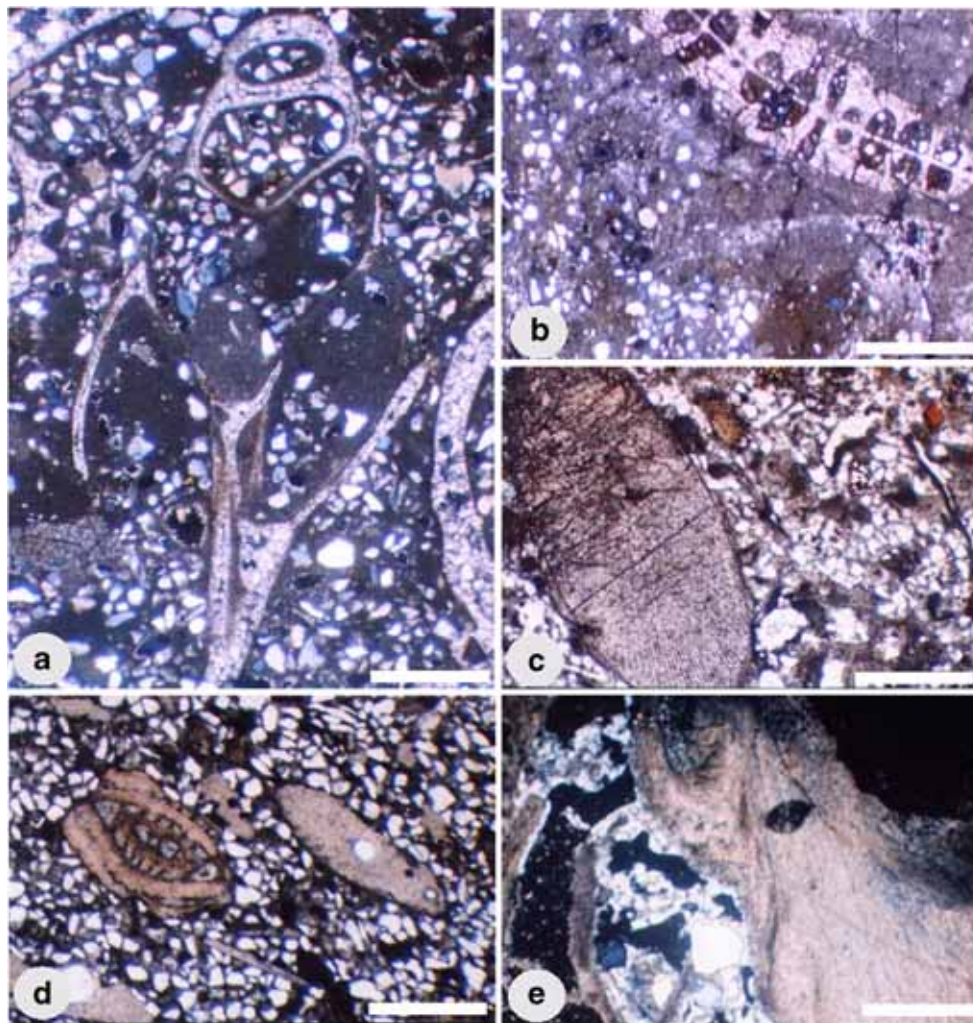
Intertidal to supratidal facies association (FA4) corresponds to dolomicrosparite facies type (F-9). It corresponds to greenish-gray, very hard, and non-fossiliferous dolostone (~6 m in thickness). This facies consists mainly of medium- to fine-grained dolomite rhombs ranging in size between 15 and 25 μm (Fig. 8d). Such dolomite crystals occur as euhedral rhombs with light peripheries, but elsewhere these are subhedral and anhedral crystals. Most of these dolomite rhombs have dark cores with argillaceous matter and clear outer rims. The dolomite rhombs are closely packed showing an equigranular, xenotopic, and hypiodotopic fabric. The matrix consists mainly of dense argillaceous matter. F-9 probably was formed in an intertidal to supratidal environment. The presence of fine-grained dolomite crystals indicates intensive evaporation of marine water in shallow intertidal and supratidal zones during short periods of sea level fall and contemporaneous replacement of previously deposited lime–mudstone (Wilson 1975; Tucker and Wright 1990; Flügel 2004).

The *Wastani Formation* is exposed in the western fringes of the Nile Delta. At Kafr Dawood Village, the Wastani Formation attains a thickness of 1.9 m, and it is represented by sand and conglomerate intercalations, mostly composed of quartz pebbles and chert nodules cemented by coarse sand and clay and covered by a 1.5-m-thick brown silt and sandy soil bed (Fig. 9a). Further west, the formation is represented by 22 m of coarse sands including a black clay bed near the top. West of the Abu Sir Pyramids, the Wastani Formation overlies unconformably the Kafr El-Shiekh Formation, while the Kom El-Shelul Formation is missing. Here, the Wastani Formation embraces 10 m thick of sands with root casts and hard ferruginous sandstone pockets. At west Dahshour, the Wastani Formation is composed of sand with minor clay intercalations (6.5 m) and overlies the Kafr El-Shiekh Formation with a marked disconformity surface in-between. At Sidmant El-Gebel Village, the sands of the Wastani Formation are ~ 15 m in thickness and are quarried actively (Fig. 9b). At Khorshed Village, this formation consists of a 18-m-thick

Fig. 8 Facies types recognized in the Kom El-Shelul Formation (continued). **a** Calcareous quartz-arenite (F-7), P.P.L., X = 33, scale bar = 1 mm. **b** Argillaceous dolostone (F-9) showing equigranular xenotopic and hypiodotopic fabric, P.P.L., X = 120, scale bar = 1 mm. **c** Nummulitic ferruginous quartz-arenite (F-7), P.P.L., X = 33, scale bar = 1 mm. **d** Dolostone (F-9) showing equigranular xenotopic and hypiodotopic fabric, P.P.L., X = 120
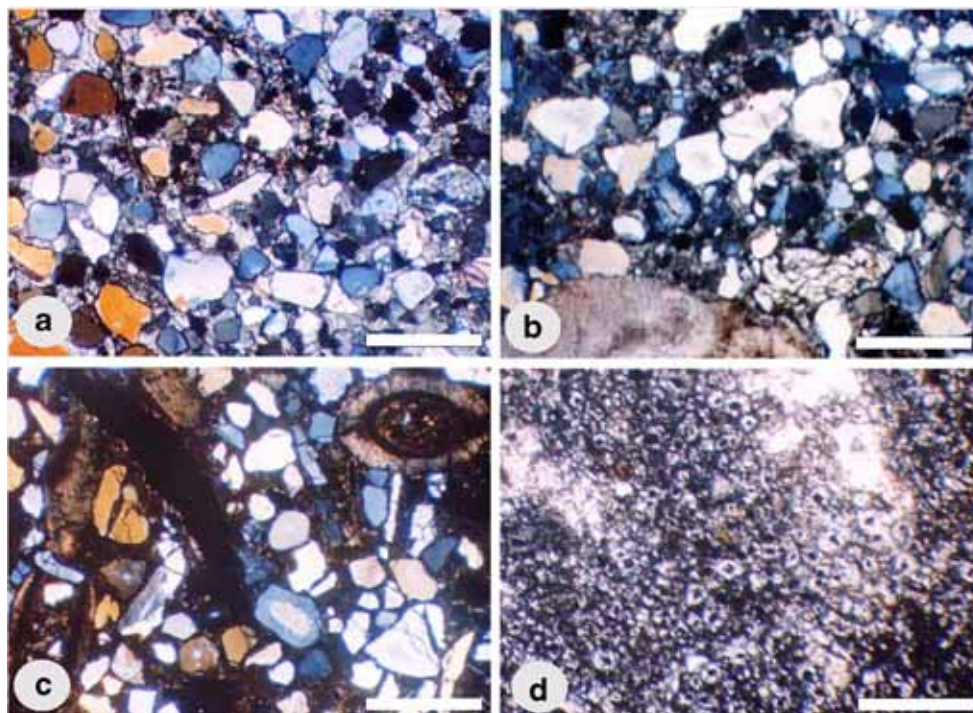
alternation of tabular sandstones and clays (Fig. 9c). It is covered by Quaternary gravels and gypsum deposits. The Wastani Formation was dated as Late Pliocene (Piacenzian) (Schlumberger 1984).

The Wastani Formation consists of alluvial facies association (FA5) with two facies types, cross-bedded sandstone (F-10), and clast-supported conglomerate (F-11) (Fig. 2).

Cross-bedded sandstone (F-10) is composed of fine- to medium-grained, light gray to grayish-yellow, moderately sorted sandstone. The sandstone beds show sheet-like geometry and planar cross-bedding, while some of them exhibit horizontal lamination. This microfacies consists mainly of fine-grained, well- to moderately sorted, monocrystalline quartz (> 98%) (Fig. 10a). Quartz grains are subangular to subrounded. They exhibit normal extinction. Feldspar grains (< 0.5%) are also recorded. Feldspars are mainly plagioclase and microcline. The cement is mainly represented by quartz overgrowths. Some grains are compacted with concavo-convex contacts in-between.

Clast-supported conglomerate (F-11) consists mainly of granule-sized, moderately sorted, rounded to subrounded, elongated, and discoidal clasts embedded into a sandy/clayey matrix. The conglomerates show massive chaotic clast fabric with occasional clast imbrication. This microfacies is composed of oligomictic conglomerate of coarse, rounded to subrounded, ill-sorted quartz grains forming 95% of the rock (Fig. 10b). Monocrystalline quartz grains represent > 85% of total quartz grains, while polycrystalline quartz grains constitute < 15%. Most of quartz grains show wavy extinction. Feldspar grains are also recorded (1%) and include

plagioclase, microcline, and albite with cloudy appearance. There are also interstitial mica flakes and brownish clay mineral or chlorite (2%). These detrital components are cemented by interstitial fine-grained quartz and micaceous clays forming about ~3% of the rock.

The present sedimentary structures and the absence of marine fossils suggest that the Wastani Formation is of fluvial origin and displays features of high-energy, low-sinuosity, braided rivers (Miall 1978). This facies association is typical for amalgamated braided stream channel fills reflecting low-accommodation conditions (Catuneanu et al. 2006). This interpretation is indicated by the cross-bedded sandstones, which are mostly the product of downstream accreting, channel bedforms (Miall 1996). The occurrence of clast-supported, lenticular, moderately sorted conglomerates implies in-channel gravel lags deposited from ephemeral braided stream (Miall 2010). The lenticular bedding of sandstones and clays formed during periods of slack water when finely suspended mud deposited at low current velocities (Reineck 1967; Reineck and Wunderlich 1968).

Quaternary

Several units of the Quaternary deposits have been distinguished in the study area. These units (1–7) are briefly described below, from the oldest to the youngest. Unit 1 is gypsum deposits present at different elevations (between 30 m and 70 m a.s.l.) in north Sidmant El-Gebel and Girza (Fig. 1). Generally, gypsum is not clean as is rich in rounded to subangular chert and limestone gravels. Unit 2 is higher gravel

Fig. 9 The Late Pliocene deposits of the study area. **a** Panoramic view of the sand beds of the Wastani Formation (Kafr Dawood quarry). **b** The Wastani Formation in the sand quarry (Sidmant El-Gebel). **c** Tabular bedding of calcareous clay bands and very fine-grained sands of the Wastani Formation (Khorshed Village)

terrace (6 m thick) mapped southward of Zawiet Dahshour and westward of Birqash (Fig. 1) in exposures located between 65 m and 75 m a.s.l. It bears pebbles of quartz, diorites, basalts, cherts, and siliceous limestones embedded into dark-red, very coarse-grained sand matrix (Fig. 11a). Unit 3 is a middle gravel terrace (6.5 m thick) found at Bedif Village (elevation of 50 m a.s.l.). The terrace includes angular to subrounded chert and limestone gravels and rare quartz pebbles, and it also bears rich shell fragments embedded into red clayey sand matrix (Fig. 11b). Unit 4 is a lower gravel terrace lies at 35 m a.s.l. to the northeast of the Maidom Pyramid. The terrace is formed of 7 m of sands with subrounded to subangular pebbles and cobbles of granites, granodiorites, quartz, cherts, and limestones (Fig. 11c). The matrix is generally ferruginous sands. Unit 5 is an alternation of gray to black, partly laminated clays and yellowish-brown, cross-bedded sands found between 25 m and 40 m a.s.l. at three localities, namely Zawiet Dahsour (thickness of 10 m), Tama Faiyum (thickness of 6.0 m), and Girza (thickness of 6.0 m). Unit 6 is formed by 8 m of fine-grained, gray to faint-yellow sands and silts, which are recorded at 30 m a.s.l. to the west of Abu Sir. The sequence includes very hard sandstone boulders and root casts. Unit 7 corresponds to sand dunes at El-Khatatba area that spill over the scarps. Small sand dunes cover the floors of the wadis to the northwest of Abu Sir Village. The approximate thickness of these deposits is 10 m.

The Quaternary sedimentation in the study area resulted from aggradation and degradation in the Nile Valley and in the nearby Fayium depression as well. The Late Pliocene regression left several isolated saline ponds on the peripheries of the gulf in topographic low basins. Severe evaporation associated with no recharge of these low basins led to the formation of gypsum deposits (unit 1). Where no topographic lows existed, erosion resulted in formation of rock-cut terraces (units 2–4). The terraces are classified according to their heights above sea level. The constant lowering of the surface between the Eastern and Western deserts happened, and the buried sediments of the former paleogulf were easily eroded and deflated more than the scarps. Though these latter scarps were also eroded and retreated as a result of the Nile Valley growth. The clay and sand unit (unit 5) is probably related to the Nile floods extending east and west at elevations between 25 and 40 m a.s.l. The sand and silt unit (unit 6) reflects also an aeolian input of sediments. Sand dunes (unit 7) are of aeolian origin.

Sand provenance

Sands of the Upper Pliocene Wastani Formation and the Quaternary units were sampled at six localities of the study area, namely Abu Sir Village (I), Kafr Dawood area (II), El-Khatatba area (III), the bench mark of 120 km of the Cairo–Alexandria road (IV), Birqash area (V), and Tahma area (VI). The locality I represents the Quaternary sands, and the localities II–VI represent the Wastani Formation.

Light minerals are quartz (95%) and feldspars (5%). *Quartz* varies from colorless and dull-yellow to reddish color. This reddish color may be attributed to a thin coat film of iron oxides around the grain surface or concentrated along fractures. Quartz grains occur as subangular to subrounded grains and show a high to medium sphericity index based on the scale of Powers (1953). The majority of quartz grains are monocrystalline, and they display a parallel to slightly undulose extinction. Inclusions are common and represented by vacuoles, zircon microcrystals, and rutile needles.

Fig. 10 Facies types recognized in the Wastani Formation. **a** Fine- to medium-grained quartz-arenite (F-10) showing graded-bedded texture (coarser grains at base and finer upwards), P.P.L., X = 33, scale bar = 1 mm. **b** Clast-supported conglomerate (F-11) consists of coarse, rounded to subrounded, ill-sorted quartz grains, P.P.L., X = 33, scale bar = 1 mm
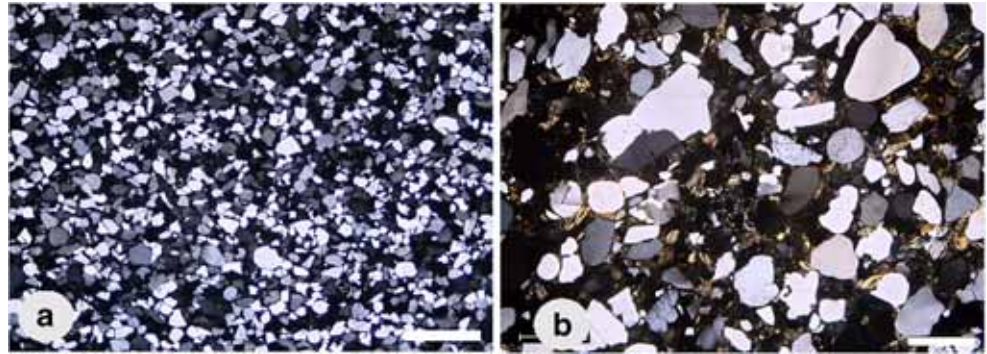
Feldspars occur as subangular to subrounded grains of pla-gioclase and orthoclase varieties. Microcline is rarely present in some investigated samples. Feldspar grains are mainly al-tered, cloudy grains that occasionally display marked twining (simple and lamellar twining).

Opaque and non-opaque fractions represent *heavy minerals* recorded in the studied samples. The investigation of these heavy mineral assemblages reveals the presence of opaque minerals, amphiboles, epidotes, garnet, zircon, pyroxenes, staurolite, rutile, tourmaline, kyanite, sphene, and biotite. Tables 2 and 3 and Figs. 12, 13, 14, and 15 show their distri-bution. *Opaque minerals* are the most abundant of the entire heavy minerals present. These are recorded in all investigated samples (Tables 2 and 3). Opaque minerals are represented mainly by iron oxide minerals (hematite, ilmenite, magnetite, and goethite). They occur in grains with different degree of roundness. Non-opaque heavy minerals include epidote, am-phiboles, garnet, zircon, rutile, staurolite, pyroxene, tourma-line, kyanite, sphene, and biotite (Fig. 16). *Epidote* is the most common non-opaque mineral (Table 2). This occurs as equidimensional subangular to subrounded grains of charac-teristic greenish-yellow color (Fig. 16a). The majority of epi-dote grains exhibit high-order interference colors.

The investigations of light and heavy fractions of sands of the Wastani Formation and Quaternary units permit some in-ferences relevant to sand provenance. The majority of quartz grains are of monocrystalline type (Conolly 1965) showing parallel extinction. Such grains belong to the common type

Fig. 11 The Quaternary deposits of the study area. **a** The higher gravel terrace (unit 2, south of Zawiet Dahshour). **b** The middle gravel terrace (unit 3, Bedif Village). **c** The lower gravel terrace (unit 4) composed of well-rounded granite and other basement gravels (to the north of the Maidom Pyramid)
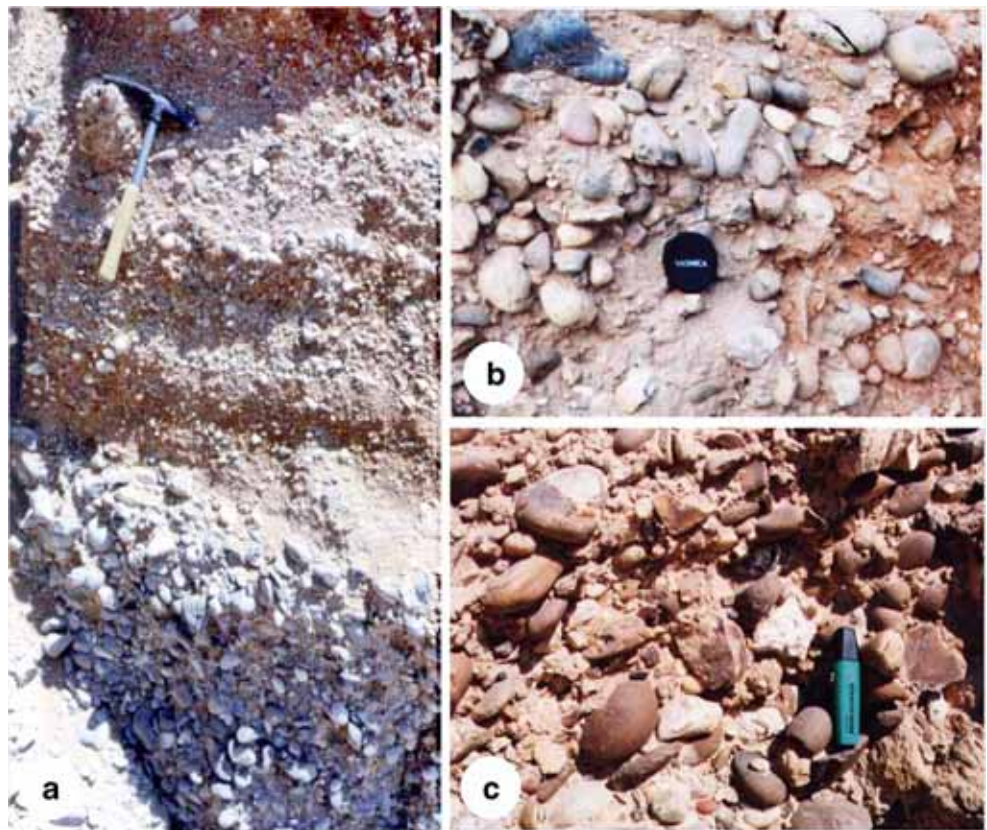
Table 2 Frequency distribution percentage of opaque and non-opaque heavy minerals recorded in the studied samples (fine and very fine-grained sand fractions, 250–63 μm). Localities: (I) Abu Sir Village, (II) Kafr Dawood area, (III) El-Khatatba area, (IV) bench mark of 120 km of the Cairo–Alexandria road, (V) Birqash area, (VI) Tahma area

Rock unit	Locality	Sample number	Opaques, %	Non-opaques, %	Non-opaques, %										
					Amphiboles	Pyroxenes	Epidote	Zircon	Garnet	Rutile	Tourmaline	Staurolite	Kyanite	Sphene	Biotite
Quaternary sand	(I)	16	61.79	38.21	9.02	18.24	22.78	7.62	9.14	9.68	8.36	4.41	8.73	1.00	1.02
		22	59.91	40.09	8.52	17.24	19.28	9.12	6.64	11.18	6.86	5.91	10.23	2.50	2.52
		23	50.27	49.73	12.67	22.42	19.71	6.72	5.39	10.41	9.63	3.64	6.54	1.50	1.37
		26	43.24	56.76	25.60	23.01	25.8	4.17	4.76	1.19	2.98	7.14	3.56	0.77	1.02
		29	71.62	28.38	20.92	25.14	12.51	7.90	15.40	3.17	4.50	4.80	3.18	1.9	0.58
The Wastani Formation (Late Pliocene)	(II)	206	63.59	36.41	20.26	7.89	18.74	9.20	15.44	8.15	5.07	6.01	2.28	4.82	2.14
		209	58.46	41.54	22.21	9.04	21.36	12.6	11.87	4.24	3.14	7.12	4.05	2.95	1.42
		214	70.63	29.37	23.29	5.89	19.37	10.48	18.35	5.40	5.01	4.20	3.94	2.82	1.25
		216	68.12	31.88	19.67	6.78	18.23	9.25	13.36	9.16	5.66	5.28	6.87	3.01	3.03
	(III)	185	69.29	30.71	16.84	10.94	21.05	8.53	11.19	8.14	6.17	6.46	6.56	2.78	1.34
		187	69.02	30.98	18.02	8.12	16.49	9.45	12.27	8.91	8.02	7.04	7.46	2.56	1.66
	(IV)	195	63.41	36.59	20.99	8.76	21.68	10.44	14.33	7.74	4.69	4.25	4.59	1.30	1.23
		196	56.24	43.76	21.49	6.26	23.68	8.94	15.83	6.24	5.19	3.75	5.09	1.80	1.73
	(V)	174	52.08	47.92	23.15	9.92	19.15	9.14	13.92	7.43	6.16	3.93	4.69	1.38	1.13
	(VI)	98	46.37	53.63	24.83	16.99	32	3.27	7.8	3.96	3.268	6.5	1.30	0.082	0.00
		99	54.2	45.80	25.35	15.72	31.7	7.52	6.34	2.82	4.224	2.11	2.81	0.003	1.41
		100	56.76	43.24	21.59	13.05	29.8	4.17	10.76	4.19	3.976	7.14	3.571	0.037	1.716

Table 3 Average frequency percentage of opaque and non-opaque heavy minerals recorded in the studied localities: (I) Abu Sir Village, (II) Kafr Dawood area, (III) El-Khatatba area, (IV) bench mark of 120 km of the Cairo–Alexandria road, (V) Birqash area, (VI) Tahma area

| Rock unit	Locality	Opaques, %	Non-opaques, %	Non-opaques, %										
				Amphiboles	Pyroxenes	Epidote	Zircon	Garnet	Rutile	Tourmaline	Staurolite	Kyanite	Sphene	Biotite
Quaternary sand	(I)	57.366	42.634	15.346	21.21	20.016	7.106	8.266	7.126	6.466	5.18	6.448	1.534	1.302
Sand of the Wastani Fm. (Late Pliocene)	(II)	65.20	34.80	21.36	7.4	19.43	10.37	14.76	6.74	4.72	5.65	4.21	3.4	1.96
	(III)	69.155	30.845	17.43	9.53	18.77	8.99	11.73	8.53	7.09	6.75	7.01	2.67	1.5
	(IV)	59.825	40.175	21.24	7.51	22.68	9.69	15.08	6.99	4.94	4.00	4.84	1.55	1.48
	(V)	52.08	47.92	23.15	9.92	19.15	9.14	13.92	7.43	6.16	3.93	4.69	1.38	1.13
	(VI)	52.44	47.56	23.925	15.254	31.17	4.99	8.35	3.58	3.821	5.26	2.56	0.04	1.05
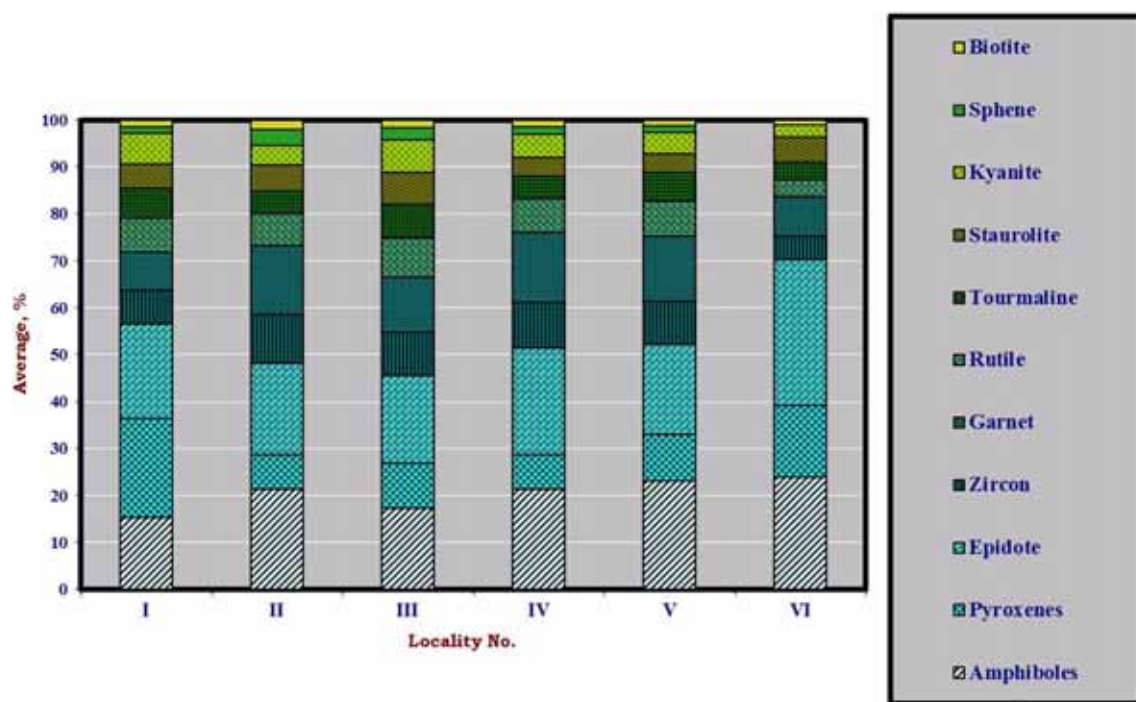
Fig. 12 Vertical distribution for the average frequency of opaque and non-opaque minerals recorded in the Wastani and Quaternary sediments in the studied localities

of Folk (1968) and thought to be derived from some disintegrated plutonic igneous rocks. Composite and semi-composite grains with slightly undulose extinction are not common. Feldspars occur in the studied samples in little portion. This can be attributed to the removal of feldspars during long transportation, as feldspars are physically and chemically weaker than quartz since they contain two sets of cleavage. The presence of microcline indicates either plutonic or metamorphic rocks (or both) as source rocks. The relative enrichment of epidotes, as well as zircon in the investigated sediments may give an indication on their derivation from basic

and intermediate igneous rocks (Maria and Heinz 1992). As shown earlier, the dominance of epidotes indicates that these deposits are of fluvial origin (Shukri and El Ayouti 1953). It should be stated here that no connection was yet established between the Egyptian river systems and those of Ethiopia or Central Africa (Issawi and Mc Cauley 1992, 1993). Therefore, these deposits are interpreted to be derived from either the Nubian Sandstone in southeastern Egypt (Coniacian–Santonian in age) or from the nearby Eocene and Oligocene sedimentary rocks, in addition to the contribution of the
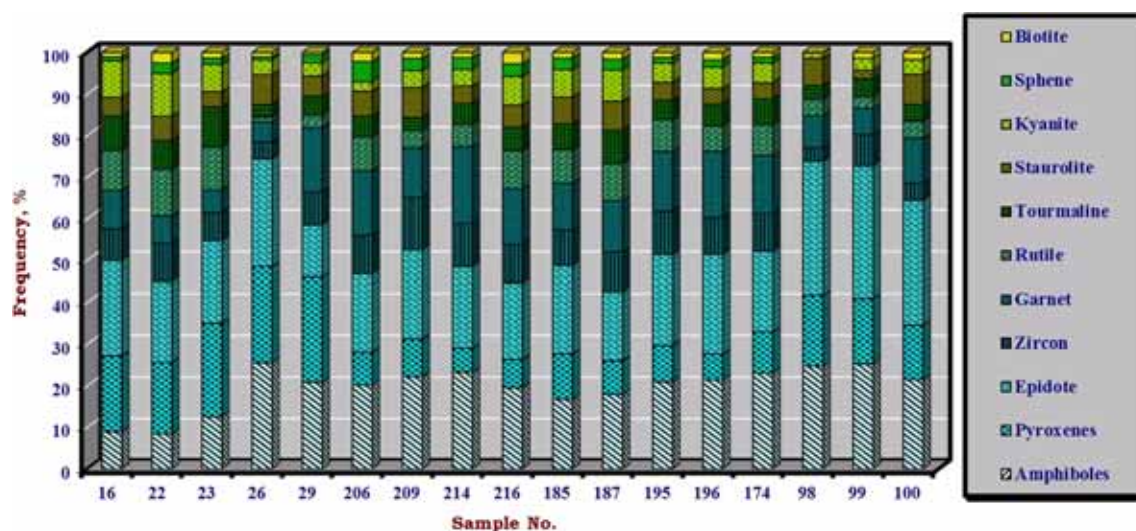

Fig. 13 Frequency distribution of opaque and non-opaque minerals recorded in the studied Wastani and Quaternary samples
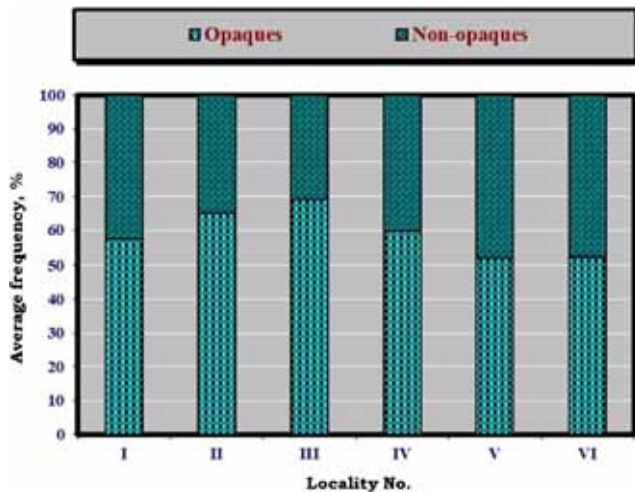
Fig. 14 Vertical distribution of the average frequency of non-opaque minerals recorded in the Wastani and Quaternary sediments in the studied localities

uncovered crystalline basement complex cropped out in the Eastern Desert.

According to Hubert (1971), the abundance of metastable (amphiboles and epidote) and ultrastable minerals (zircon, rutile, and tourmaline) indicates a metamorphic source. The presence of biotite and monocrystalline quartz results from the contributions of plutonic igneous rocks, whereas rounded to subrounded grains of zircon, rutile, and tourmaline could be derived from some reworked deposits. In our case, the source area is thought to be the Egyptian Eastern Desert where both metamorphic and sedimentary rocks are most common. Pyroxenes were driven, most probably, from the Qatrani basalt

in Faiyum and also from the basalts of the Bahnassa area (28° 30′ N and 30° 32′ E) and the Eastern Desert. The relative increase in the amount of pyroxenes in the Quaternary sands indicates, probably, the basaltic derivation from Ethiopia when the welding of both the Atbara River and the Blue Nile with the Egyptian Nile occurred in the Early–Middle Pleistocene.

Discussion

Sedimentary evolution

The documented stratigraphical sequence of facies associations (Fig. 17) implies the marine incursion into the study area occurred in the beginning of the Pliocene. The appeared paleogulf was relatively deep-water (FA-1). Its shallowing started already in the Zanclean when subtidal, intertidal, and supratidal depositional environments and later deltaic depositional environments established (FA-2–4). This trend culminated in the Piacenzian (Late Pliocene) when fluvial accumulation restored (FA5). However, the shoreline was located closely to the study area because excessive evaporation resulted in gypsum accumulation in saline ponds (Quaternary unit 1) yet in the beginning of the Pleistocene. Later, the modern Nile valley and delta evolved. Where no topographic lows existed, erosion resulted in formation of rock-cut terraces (units 2–4). The clay and sand (unit 5) is probably related to the Nile floods extending east and west at elevations between 25 and 40 m a.s.l. Unit 6 (sand and silt) is admixture of aeolian action with interdegitated Nile silt. The sand and silt unit (unit
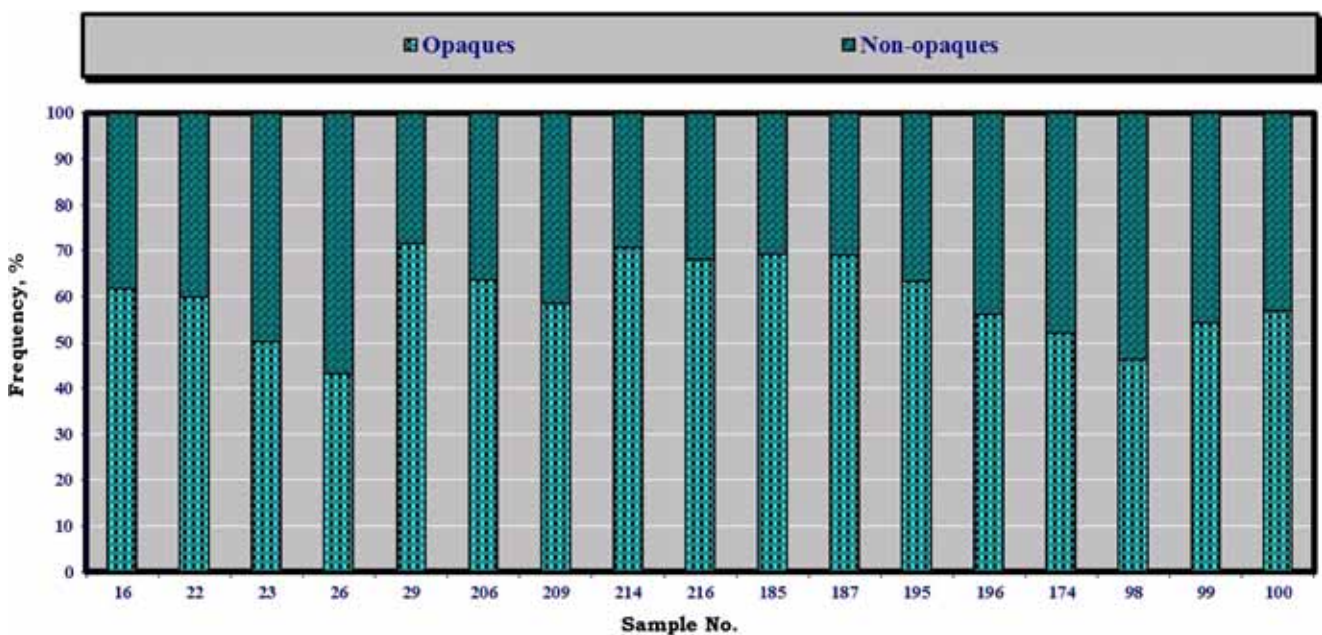

Fig. 15 Frequency distribution of the non-opaque minerals recorded in the Wastani and Quaternary samples

Fig. 16 Heavy mineral association recorded in the Pliocene and Quaternary deposits of the study area. **a** Epidote grain, P.P.L., X = 160. **b** Amphibole grain, P.P.L., X = 160. **c–e** Garnet grains, sometimes display criss-cross mamillated surface, P.P.L., X = 160. **f–h** Zircon grains with inclusions, P.P.L., X = 160. **i, j** Rutile grains, X = 160. **k, l** Staurolite grains, X = 160. **m, n** Pyroxene grains, X = 160. **o** Tourmaline grain, C.N., X = 160. **p** Kyanite grain, C.N., X = 220
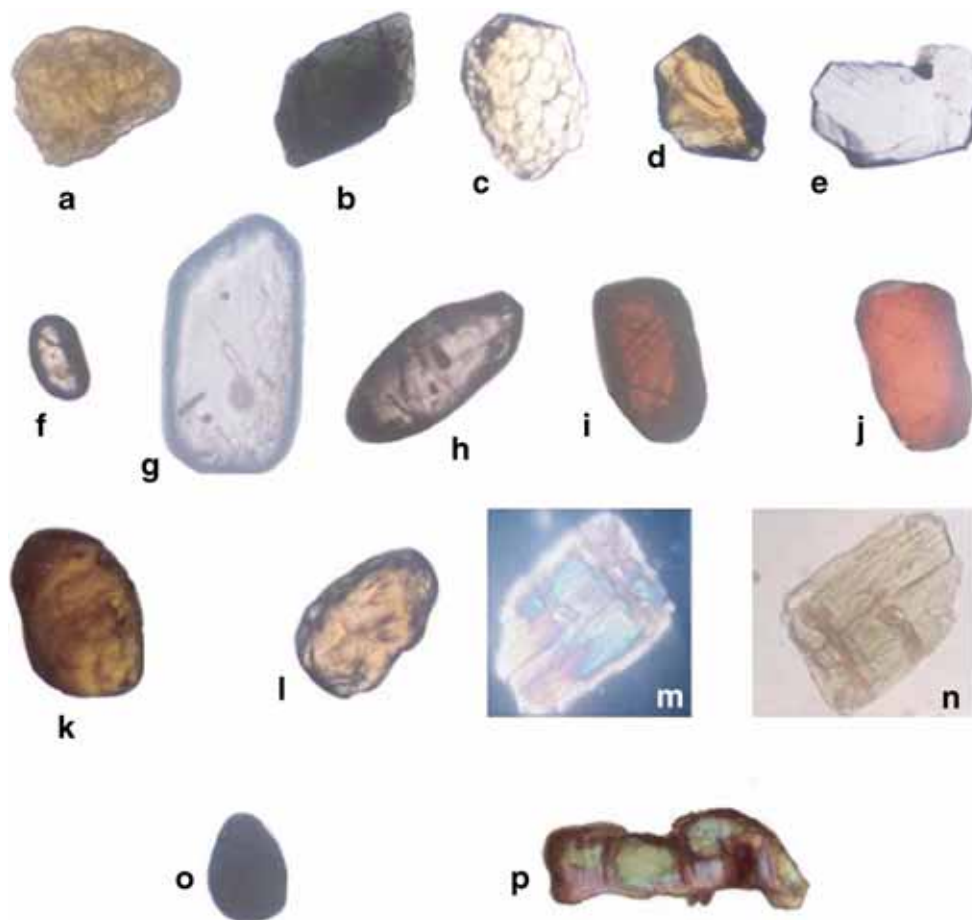
6) points to also an aeolian input of sediments. Sand dunes (unit 7) are of aeolian origin.

Generally, the Early Pliocene (Zanclean) was a particular phase in the evolution of the Nile Delta. The development of the latter can be described as a rapid marine incursion with formation of the Nile Paleogulf followed by its gradual retreat. As the Nile Valley was developed, most probably, before the Pliocene (Fielding et al. 2018), the paleogulf was formed via marine flooding of the pre-existing valley, which explains its elongated view on the paleogeographic reconstructions of Guiraud et al. (2005) and Abdelsalam (2018). The latter specialist terms this paleogeographic features as the "Eonile Canyon-Gulf." The Late Pliocene (Zanclean)–Quaternary phase is relevant to the evolution of the riverine valley.

Paleoenvironmental context

The registered paleogulf appearance and disappearance requires interpretation in the broad paleoenvironmental context. Principally, it should be understood why the marine incursion was so rapid that led to the flooding of the former valley (see Abdelsalam (2018) for discussion of the relationship of this valley to the modern Nile). Prior to the appearance of the discussed paleogulf, the Mediterranean experienced significant environmental perturbations. The so-called Messinian Salinity Crisis led to the desiccation of the marine basin (or, at least, its significant parts), massive evaporite accumulation, etc.; the marine basin restored in the beginning of the Pliocene during the so-called the Zanclean Flood (Hsü et al. 1973; Ruggieri and Sprovieri 1976; Adams et al. 1977; Hsü 1978; Wright 1979; Wright and Cita 1979; Gautier et al. 1994; Krijgsman et al. 1999; Duggen et al. 2003; Loget et al. 2005; Roveri and Manzi 2006; Suc et al. 2007; Gargani and Rigollet 2007; Rouchy et al. 2007; Garcia-Castellanos et al. 2009; Govers 2009; Perez-Asensio et al. 2013; Roveri et al. 2014, 2016; Marzocchi et al. 2016; Vai 2016; Vasiliev et al. 2017). This event strongly perturbed sedimentary complexes of the southeastern edge of the Mediterranean (Kirkham et al. 2018). It is beyond the scope of the present paper to review the salinity crisis timing and scenario, but the wide Early Pliocene transgression should be noted. Some modern data indicates this transgression could start a bit earlier (Leila et al. 2018). Reestablishment of the connection of the Mediterranean Sea with the Atlantic Ocean means that the spatial extension of the noted transgression was limited by the global sea level related to the topography of the study area. The eustatic curve proposed by Haq and Al-Qahtani (2005) who updated
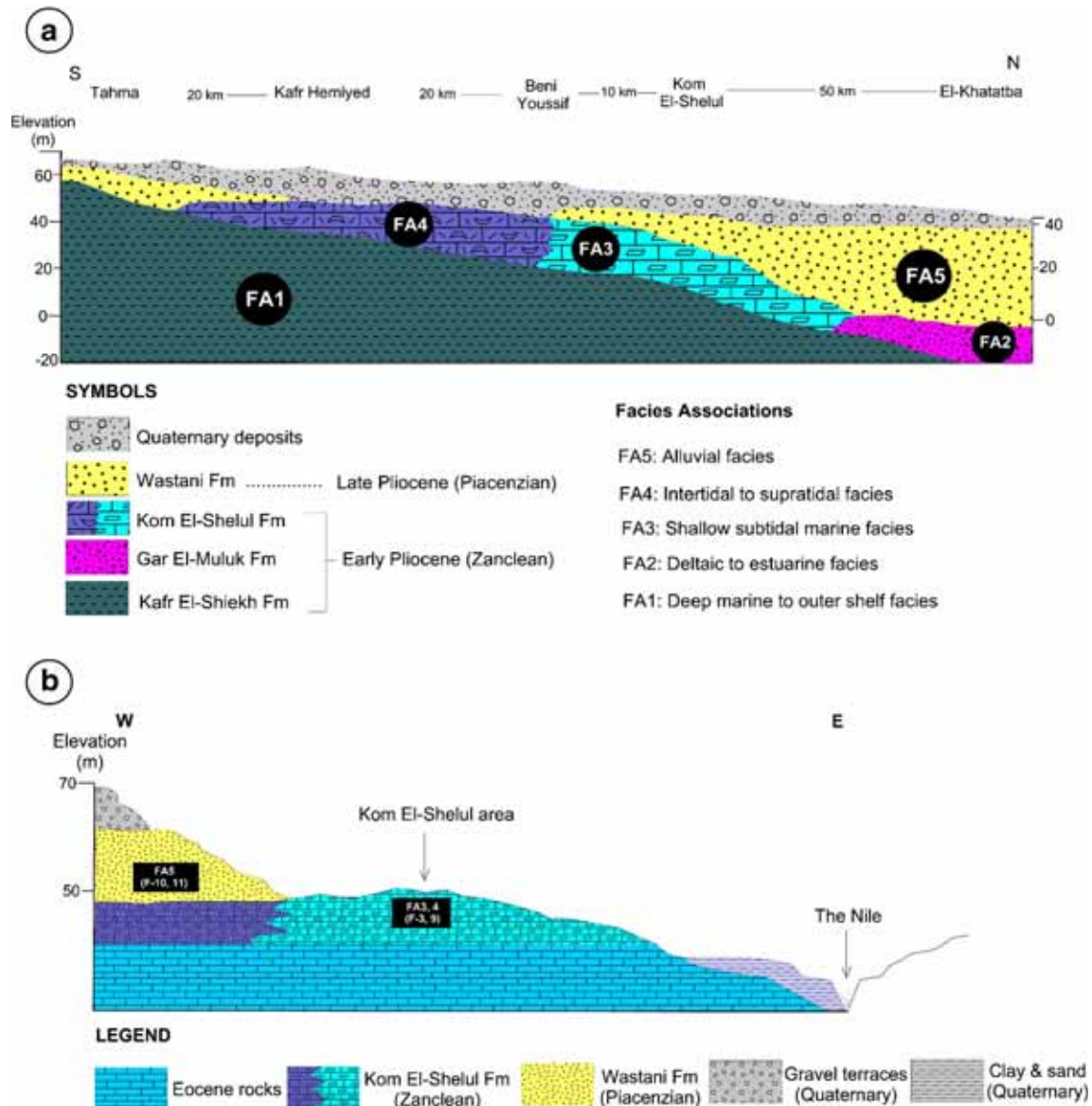
Fig. 17 Distribution of facies associations in the Pliocene–Quaternary sediments across the study area. **a** N–S cross section. **b** W–E cross section

the earlier curve by Haq et al. (1987) implies that the global sea level in the Zanclean was significantly lower than in the Oligocene–Miocene when fluvial deposition already dominated on the study area. The alternative eustatic reconstruction proposed by Miller et al. (2005) shows higher global sea level in the Zanclean; but this level was anyway lower than in the Eocene, which was the last epoch of marine deposition on the study area (Fig. 2). If so, a significant marine incursion in the Nile Delta region in the Zanclean triggered by the only sea level rise associated with "the Zanclean Flood" seems to be impossible. However, the low level of the Mediterranean Sea before the reestablishment of its connection to the Atlantic Ocean might have triggered significant incision of the Nile Valley, as a result

of which this valley became deeper than before the Messinian Salinity Crisis (see review in Said 1993; Abdelsalam 2018). The flooding of the desiccated Mediterranean and the moderately high global sea level coupled with the increase in the local accommodation space because of the noted incision were able to result in the appearance of the Nile Paleogulf.

The factor of local tectonic activity played a merely negative than positive role in the paleogulf development. The study area was located closely to the opened Red Sea and its northern branches, and, thus, it experienced relevant uplift (Guiraud et al. 2005). This uplift reduced the accommodation space since the Oligocene. A significant regional-scale subsidence appears to be impossible. In contrast, the

regional uplift could cause the beginning of the paleogulf retreat already in the middle Zanclean. Because of warming, the global sea level experienced some significant rises in this time (Haq and Al-Qahtani 2005; Miller et al. 2005; Dwyer and Chandler 2009; Raymo et al. 2011; Rovere et al. 2014). However, the gradual seaward shoreline shift in the southwestern fringes of the Nile Delta continued. The role of the regional uplift is stressed by the results of the undertaken analysis of the provenance of the Wastani sands. These results indicate sediment delivery to the study area from the nearby territories of Egypt. If so, the intensive erosion of the uplifted domain should be interpreted. Additionally, voluminous deposition of the siliciclastic material led to quick filling of topographical lows, which reduced the accommodation space (cf. Said 1993; Abdelsalam 2018). As a result, the paleogulf disappeared gradually together with fluvial system progradation. Of course, the rise of the ice sheets in the both hemispheres and the relevant global sea level fall (Zachos et al. 2001; Haq and Al-Qahtani 2005; Miller et al. 2005) also contributed to the final disappearance of the Nile Paleogulf to the end of the Pliocene.

This study is also detailed enough to discuss paleoenvironmental changes in the study area. The N–S cross section demonstrates that the Kafr El-Shiekh Formation representing the main stage of the Nile Paleogulf development (rapid marine incursion and flooding of pre-existing gorge) has maximum distribution (Fig. 17a). Late, at the time of the deposition of the Gar El-Muluk Formation, the paleogulf retreated, but it quickly extended once again in the late Zanclean when carbonates of the Kon El-Shelul Formation were formed (Fig. 17a). Most probably, this dynamics should be explained in the terms of the global sea level changes (Haq and Al-Qahtani 2005; Miller et al. 2005) that triggered pronounced shoreline shifts on generally "flat" surfaces. This surface developed in the Nile Delta when the pre-Pliocene gorge was filled completely with the deposits now constituting the Kafr El-Shiekh Formation. Special attention should be paid to alluvial sands of the Wastani Formation. Most probably, these are absent in the central part of the study area (Fig. 17a) because of erosion or denudation by river channels in the Quaternary times. Their bigger thickness in the north of the study area can be explained logically by the existence of topographic low in the lowermost part of the delta, which increased accommodation space and, thus, allowed more sediments to accumulate. The W–E cross section shows that the principal paleoenvironmental changes occurred along the Nile Valley and not across it (Fig. 17b). The both early and late Zanclean marine facies embrace the area from the Nile to the west border of its valley. Generally, the relationship of the facies associations (Fig. 17) confirms quick growth of N–S trending of the Nile Paleogulf that later disappeared because of sedimentary filling. This paleogulf inherited a pre-Pliocene river valley, and this valley restored after paleogulf filling.

Conclusions

The new investigations of the Pliocene–Quaternary sedimentary succession in the southwestern fringes of the Nile Delta permits making five general conclusions:

1. The Kafr El-Shiekh, Gar El-Muluk, and Kom El-Shelul formations constitute the lower (Zanclean) part of the Pliocene sedimentary sequence, and the Wastani Formation constitutes its upper (Piacenzian) part.
2. The deep marine to outer shelf, deltaic to estuarine, shallow subtidal marine, intertidal to supratidal, and alluvial facies associations are established in the Pliocene–Quaternary sedimentary succession.
3. The undertaken provenance analysis of Pliocene–Quaternary sands indicates various but chiefly nearby sources of detrital particles.
4. The stratigraphical sequence of the facies associations indicates the rapid marine incursion and paleogulf formation in the beginning of the Zanclean and the gradual paleogulf retreat in the middle–late Zanclean, whereas fluvial deposition dominated the Piacenzian–Pleistocene.
5. The Nile Paleogulf evolution was controlled by a kind of coincidence of regional and global factors including the global sea level changes relevant to the Late Cenozoic ice sheet dynamics, the Messinian Salinity Crisis, the tectonic uplift, and the changes in the accommodation space.

References

Abd El Shafy E, Metwally MHM (1986) Stratigraphy of the Pliocene series in the northern part of the Nile Valley, Egypt, 1-Macrostratigraphy, Bull Fac Sci Zagazig Univ 8:106–141

Abd El Shafy E, Hamza F, Metwally MHM (1987) Stratrigaphy of the Pliocene series in the northern part of the Nile Valley, Egypt. 2-Lithostratigraphy and paleoenvironments: Bull Fac Sci, Zagazig Univ 9:426–456

Abdallah AY (1970) Petrology of some Pliocene recent rocks in Wadi El Natrun–Beni Suef area, Egypt. M.Sc. Thesis, Fac. Sci. Ain Shams Univ., 187p

Abdelsalam MG (2018) The Nile's journey through space and time: a geological perspective. Earth Sci Rev 177:742–773

Adams CG, Benson RH, Kidd RB, Ryan WBF, Wright RC (1977) The Messinian Salinity Crisis and evidence of late Miocene eustatic changes in the world ocean. Nature 269:383–386

Adamson DA, Gasse F, Street FA, Williams MAJ (1980) Late Quaternary history of the Nile. Nature 288:50–55

Baloge P-A, Brosse R (1993) New stratigraphical and paleogeographical data on lowermost Liassic from southwest of the Paris Basin; evidence of an Hettangian paleogulf in Anjou. Geologie de la France 1: 57–60

Barr FT, Walker BR (1973) Late Tertiary channel system in northern Libya. In: Ryan W, Hsu K (eds) Initial reports of the Deep Sea Drilling Project, vol 13. U.S. Government Printing Office, Washington, pp 1244–1251

Blanckenhorn M (1921) Handbuch der regionalen geologie, bd., vii, abt. 9, Heft 23, Agypten. Heidelberg, 244p

Catuneanu O, Khalifa MA, Wanas HA (2006) Sequence stratigraphy of the Lower Cenomanian Bahariya Formation, Bahariya Oasis, Western Desert, Egypt. Sediment Geol 190:121–137

Chumakov IS (1967) Pliocene and Pleistocene deposits of the Nile Valley in Nubia and Upper Egypt (in Russian). Trans Geol Inst Acad Sci (USSR) 170:1–110

Chumakov IS (1968) Pliocene ingression into the Nile Valley according to new data. In: Butzer KW, Hansen CL (eds) The desert and river in Nubia. University of Wis Consin press, Madison, pp 521–523

Chumakov IS (1973a) Geological history of the Mediterranean at the end of the Miocene—the beginning of the Pliocene according to new data. In: Ryan W, Hsü K et al (eds) Initial reports of deep sea drilling project, vol 13. U.S. Government Printing Office, Washington 1241p

Chumakov IS (1973b) Pliocene and Pleistocene deposits of the Nile Valley in Nubia and Upper Egypt. In: Ryan W, Hsü K et al (eds) Intial reports of deep sea drilling project, vol 13. U.S. Government Printing Office, Washington 1242p

Conolly JR (1965) The occurrence of polycrystallinity and undulatory extinction in quartz in sandstones. J Sediment Petrol 35:116–135

Didyke BM, Simoneit BRT, Brassell SC, Eglinton G (1978) Organic geochemical indicators of paleoenvironmental conditions of sedimentation. Nature 272:216–222

Dubar M (1988) The Holocene coastal transgressive series of the Nice area, a sedimentary model. Bull Assoc Francaise pour l'Etude du Quaternaire 33:11–15

Duggen S, Hoernie K, Van den Bogaard P, Rupke L, Morgan JP (2003) Deep roots of the Messinian Salinity Crisis. Nature 422:602–606

Dunham RJ (1962) Classification of carbonate rocks according to depositional texture. In: Ham WE (ed) Classification of carbonate rocks, vol 1. Okla. A.A.P.G. Mem., Tulsa, pp 108–121

Dwyer GS, Chandler MA (2009) Mid-Pliocene sea level and continental ice volume based on coupled benthic Mg/Ca palaeotemperatures and oxygen isotopes. Philos Trans R Soc A Math Phys Eng Sci 367:157–168

Embry AF, Kolven JE (1972) A late Devonian reef tract on northeastern banks Island, Northwest territories. Bull Can Petrol Geol 19:73–781

Fielding L, Najman Y, Millar I, Butterworth P, Garzanti E, Vezzoli G, Barfod D, Kneller B (2018) The initiation and evolution of the River Nile. Earth Planet Sci Lett 489:166–178

Flügel E (2004) Microfacies of carbonate rocks: analysis, interpretation and application. Springer, Berlin 976 p

Folk RL (1968) Petrology of sedimentary rocks. Hemphills Publishing Co., Texas 70 p

Fourtau R (1920) Echinodermes Neogene de L'Egypt; catalogue des invertebres follils d' Egypt: Terrains Teriates; pt. 2: Geol. Surv. Egypt, Cairo 101p

Garcia-Castellanos D, Estrada F, Jimenez-Munt I, Gorini C, Fernandez M, Verges J, De Vicente R (2009) Catastrophic flood of the Mediterranean after the Messinian Salinity Crisis. Nature 462: 778–781

Gargani J, Rigollet C (2007) Mediterranean Sea level variations during the Messinian Salinity Crisis. Geophys Res Lett 34:L10405

Gautier F, Clauzon G, Suc J-P, Cravatte J, Violanti D (1994) Age and duration of the Messinian Salinity Crisis. C R Acad Sci Ser II: Sci Terre Planets 318:1103–1109

Geologic Map of Egypt (1981) Scale 1: 2,000,000. Cairo

Govers R (2009) Choking the Mediterranean to dehydration: the Messinian Salinity Crisis. Geology 37:167–170

Gradstein FM, Ogg JG, Schmitz M, Ogg G (eds) (2012) The geologic time scale 2012, vol 1–2. Elsevier, Oxford 1176p

Guiraud R, Bosworth W, Thierry J, Delplanque A (2005) Phanerozoic geological evolution of Northern and Central Africa: an overview. J Afr Earth Sci 43:83–143

Hamdan MA (1992) Pliocene and Quaternary deposits of Beni suef–East Fayium area and their relation to the geological evolution of the River Nile. Ph. D. Thesis, Cairo Univ., 274p

Hamza F (1972) Study on some Pliocene fauna from Egypt. M. Sc. Thesis, Fac, Sci., Ain Shams Univ

Hamza F (1983) Post-Pliocene transgressive phase along the northern part of the Nile Valley, Egypt, N Jb Geol Paleont Mh, H 6

Hamza F, Metwally MHM (1984) Lithstratigraphic contribution to the Pliocene rocks at the western edge of the Nile–Fayium divide, Egypt. Bull. Fac. Sci. Zagazig Univ., Egypt, 6, no. 6

Haq BU, Al-Qahtani AM (2005) Phanerozoic cycles of sea-level change on the Arabian platform. GeoArabia 10:127–160

Haq BU, Hardenbol J, Vail PR (1987) Chronology of fluctuating sea levels since the Triassic. Science 235:1156–1167

Harms JC, Wray JL (1990) Nile Delta. In: Said R (ed) The gelogy of Egypt. Balkema, chapter 17, pp 329–343

Hassan MY, Issawi B, Zaghloul EA (1978) Geology of the area east of Beni Suef, Eastern Desert, Egypt. Ann Geol Surv Egypt 8:129–162

Hsü KJ (1978) The Messinian Salinity Crisis—evidence of Late Miocene eustatic changes in the world ocean. Naturwissenschaften 65:151

Hsü K, Cita MB, Ryan WBF (1973) The origin of the Mediterranean evaporates. In: Ryan W, Hsü K et al (eds) Initial reports of deep sea drilling project, vol 13. U.S. Government Printing Office, Washington, pp 1203–1231

Hubert JF (1971) Heavy minerals. In: Carver RE (ed) In procedures in sedimentary petrology. Willey interscience, New York 476 p

Huerta P, Armenteros I (2005) Calcrete and palustrine assemblages on a distal alluvial-floodplain: a response to local subsidence (Miocene of the Duero Basin, Spain). Sediment Geol 177:235–270

Issawi B, Mc Cauley J (1992) The Cenozoic rivers of Egypt the Nile problem. In: The followers of Horus (Eds. R. Friedman and B. Adams), Egypt. Studies Assoc. Publi., no. 2, Oxbow Monograph, 20, 121–146

Issawi B, Mc Cauley J (1993) The Cenozoic landscape of Egypt and its river system. Ann Geol Surv Egypt 19:359–384

Issawi B, Sallam ES (2017) Rejuvenation of dry palaeochannels in arid regions in NE Africa: a geological and geomorphological study. Arab J Geosci 10:14. https://doi.org/10.1007/s12517-016-2793-z

Issawi B, Hassan MY, Osman R (1978) Geological studies in the area of Kom Ombo in Eastern Desert, Egypt. Ann Geol Surv Egypt 8:187–235

Issawi B, Ahmed SM, Osman R, Sallam ES (2005) Studies on the Pliocene—Quaternary sediments in the western fringes of the Nile Delta—lower Nile Valley stretch, Egypt. Sedimentol Egypt 13:277–296

Issawi B, Sallam E, Zaki SR (2016) Lithostratigraphic and sedimentary evolution of the Kom Ombo (Garara) sub-basin, southern Egypt. Arab J Geosci 9:420. https://doi.org/10.1007/s12517-016-2440-8

Issawi B, Sallam ES, Salem M (2018) Tectonostratigraphic and sedimentary evolution of the Ubur–Orabi sub-basin, southeast Nile Delta, Eypt. Carbonates Evaporites. https://doi.org/10.1007/s13146-017-0392-z

Khonde NN, Maurya DM, Chamyal LS (2017) Late Pleistocene–Holocene clay mineral record from the Great Rann of Kachchh basin, Western India: implications for palaeoenvironments and sediment sources. Quat Int 443:86–98

Kirkham C, Cartwright J, Hermanrud C, Jebsen C (2018) The formation of giant clastic extrusions at the end of the Messinian Salinity Crisis. Earth Planet Sci Lett 482:434–445

Krijgsman W, Hilgen FJ, Raffi I, Sierro FJ, Wilson DS (1999) Chronology, causes and progression of the Messinian Salinity Crisis. Nature 400:652–655

Leila M, Moscariello A, Segvic B (2018) Geochemical constraints on the provenance and depositional environment of the Messinian sediments, onshore Nile Delta, Egypt: implications for the late Miocene paleogeography of the Mediterranean. J Afr Earth Sci 143:215–241

Loget N, Van Den Driessche J, Davy P (2005) How did the Messinian Salinity Crisis end? Terra Nova 17:414–419

Maria AM, Heinz FW (1992) Heavy minerals in colours. Chapman & Hall, London 147 p

Marzocchi A, Flecker R, van Baak CGC, Lunt DJ, Krijgsman W (2016) Mediterranean outflow pump: an alternative mechanism for the Lago-mare and the end of the Messinian Salinity Crisis. Geology 44:523–526

Mayer-Eymer K (1898) Systematiches verzeichniss der fauna des unteren Sahrianum (marine quarter) der umgegend von Kairo, nebst Bescheréibung der neuen Arten. Paleontographica, stuttgrat 30:60–90

Miall AD (1978) Lithofacies types and vertical profile models in braided river deposits, a summary. In: Miall AD (ed) Fluvial sedimentology. Canadian Society Petroleum Geologist Memoir, 5:597–604

Miall AD (1996) The geology of fluvial deposits. Springer-Verlag 582p

Miall AD (2010) Alluvial deposits. In: James NP, Dalrymple RW (eds) Facies models 4. Geological Association of Canada, St. John's Newfoundland, pp 105–137

Miller KG, Kominz MA, Browning JV, Wright JD, Mountain GS, Katz ME, Sugarman PJ, Cramer BS, Christie-Blick N, Pekar SF (2005) The phanerozoic record of global sea-level change. Science 310: 1293–1298

Negri MP (2009) An experimental mapping method by means of fossil mollusk faunas: the Holocene Thai paleogulf. Boll Soc Paleontol Ital 48:41–50

Newton RB (1899) Egyptian newer tertiary shells. Geol Mag 6:352–359

Nichols G (2009) Sedimentology and stratigraphy. Wiley-Blockwell, Chichester 419p

Odin GS (1988) Green marine clays. Dev Sedimentol 45 445p

Odin GS, Matter A (1981) De glauconiarum origine. Sedimentology 28: 611–641

Ogg JG, Ogg GM, Gradstein FM (2016) A concise geologic time scale 2016. Elsevier, Amsterdam 234p

Pennington BT, Sturt F, Wilson P, Rowland J, Brown AG (2017) The fluvial evolution of the Holocene Nile Delta. Quat Sci Rev 170:212–231

Perez-Asensio JN, Aguirre J, Jimenez-Moreno G, Schmiedl G, Civis J (2013) Glacioeustatic control on the origin and cessation of the Messinian Salinity Crisis. Glob Planet Chang 111:1–8

Pettijhon FJ, Potter PE, Siever R (1973) Sand and sandstone. Springer-Verlag New York, Heidelberg 618p

Pfeiffer M, Le Roux JP, Solleiro-Rebolledo E, Kemnitz H, Sedov S, Seguel O (2011) Preservation of beach ridges due to pedogenic calcrete development in the Tongoy palaeobay, North-Central Chile. Geomorphology 132:234–248

Platt NH, Wright VP (1992) Palustrine carbonates at the Florida Everglades: towards an exposure index for the freshwater environment. J Sediment Petrol 62:1058–1071

Powers MC (1953) A new roundness scale for sedimentary particles. J Sediment Petrol 23:117–119

Raymo ME, Mitrovica JX, O'Leary MJ, Deconto RM, Hearty PJ (2011) Departures from eustasy in Pliocene sea-level records. Nat Geosci 4: 328–332

Reineck H (1967) Layered sediments of tidal flats, beaches, and shelf bottoms of the North Sea. Estuaries 83:191–206

Reineck H, Wunderlich F (1968) Classification and origin of flaser and lenticular bedding. Sedimentology 11:99–104

Rouchy JM, Caruso A, Pierre C, Blanc-Valleron M-M, Bassetti MA (2007) The end of the Messinian Salinity Crisis: evidences from the Chelif Basin (Algeria). Palaeogeogr Palaeoclimatol Palaeoecol 254:386–417

Rovere A, Raymo ME, Mitrovica JX, Hearty PJ, O'Leary MJ, Inglis JD (2014) The Mid-Pliocene sea-level conundrum: glacial isostasy, eustasy and dynamic topography. Earth Planet Sci Lett 387:27–33

Roveri M, Manzi V (2006) The Messinian Salinity Crisis: looking for a new paradigm? Palaeogeogr Palaeoclimatol Palaeoecol 238:386–398

Roveri M, Flecker R, Krijgsman W, Lofi J, Lugli S, Manzi V, Sierro FJ, Bertini A, Camerlenghi A, De Lange G, Govers R, Hilgen FJ, Hubscher C, Meijer PT, Stoica M (2014) The Messinian Salinity Crisis: past and future of a great challenge for marine sciences. Mar Geol 352:25–58

Roveri M, Gennari R, Lugli S, Manzi V, Minelli N, Reghizzi M, Riva A, Rossi ME, Schreiber BC (2016) The Messinian Salinity Crisis: open problems and possible implications for Mediterranean petroleum systems. Pet Geosci 22:283–290

Ruban DA (2010) Stratigraphic evidence of a Late Maeotian (Late Miocene) punctuated transgression in the Tanais palaeobay (northern part of the eastern Paratethys, south-west Russia). Geologos 16: 169–181

Ruggieri G, Sprovieri R (1976) Messinian Salinity Crisis and its paleo-geographical implications. Palaeogeogr Palaeoclimatol Palaeoecol 20:13–21

Said R (1962) The geology of Egypt. El Sevier, 377p

Said R (1971) Explanatory notes to accompany the geological map of Egypt. Egypt Geol Surv 56, 123p

Said R (1993) The River Nile: geology, hydrology and utilization. Pergamon Press, New York 320 pp

Said R, Bassiouni MA (1958) Calabrian microfossils from Kom El Shelul, Giza, Egypt. Egypt J Geol 2(2)

Sallam E, Wanas HA, Osman R (2015) Stratigraphy, facies analysis and sequence stratigraphy of the Eocene succession in the Shabrawet area (north Eastern Desert, Egypt): an example for a tectonically influenced inner ramp carbonate platform. Arab J Geosci 8(12): 10433–10458

Schlumberger (1984) Well evaluation conference, Egypt. Geol Egypt 1: 471–446

Schweinfurth G (1889) Ueber dei kreideregion bei den Pyramiden von Gizeh. Petrm Mitt bd 35:1–2

Segev A, Avni Y, Shahar J, Wald R (2017) Late Oligocene and Miocene different seaways to the Red Sea–Gulf of Suez rift and the Gulf of Aqaba–Dead Sea basins. Earth Sci Rev 171:196–219

Shukri NM, El Ayouti MK (1953) The mineralogy of Eocene and later sediments in Anqabia area, Cairo – Suez district. Bull Fac Sci Cairo Univ 32:47–58

Suc J-P, Rouchy JM, Ferrandini M, Ferrandini J (2007) The Messinian Salinity Crisis revisited. Geobios 40:231–232

Tucker ME (1982) Sedimentary Petrology: An introduction. Blackwell Scientific Publications. Geoscience texts, 3 251 p

Tucker ME, Wright VP (1990) Carbonate sedimentology. Blackwell Science, Oxford 482p

Vai GB (2016) Over half a century of Messinian Salinity Crisis. Boletin Geologico y Minero 127:625–641

Vasiliev I, Mezger EM, Lugli S, Reichart G-J, Manzi V, Roveri M (2017) How dry was the Mediterranean during the Messinian Salinity Crisis? Palaeogeogr Palaeoclimatol Palaeoecol 471:120–133

Vischer A (1947) Geological reconnaissance survey of the Wadi El-Natum area, Western Desert, Egypt. Nat Res Cent Cairo, F 12

Wanas HA, Sallam E, Zobaa MK, Li X (2015) Mid-Eocene alluvial-lacustrine succession at Gebel El-Goza El-Hamra (Shabrawet area, NE Eastern Desert, Egypt): facies analysis, sequence stratigraphy and paleoclimatic implications. Sediment Geol 329:115–129

Wilson JL (1975) Carbonate facies in geologic history. Springer, New York 471p

Woodward JC, Williams MAJ, Garzanti E, Macklin MG, Marriner N (2015) From source to sink: exploring the quaternary history of the Nile. Quat Sci Rev 130:3–8

Wright RC (1979) Messinian correlation: salinity crisis. Episodes 3:12–15

Wright R, Cita MB (1979) Geo- and biodynamic effects of the Messinian Salinity Crisis in the Mediterranean. Palaeogeogr Palaeoclimatol Palaeoecol 29:215–222

Zachos J, Pagani M, Sloan L, Thomas E, Billups K (2001) Trends, rhythms, and aberrations in global climate 65 Ma to present. Science 292:686–693

Zaghloul ZM, Andrawis SF, Ayad SN (1979) New contribution to the stratigraphy of the Tertiary sediments of Kafr El-Dawar, well no. 1, NW Nile Delta, Egypt. Ann Geol Surv Egypt 9:292–307